Humans adapt their anticipatory eye movements to the volatility of visual motion properties

Chloé Pasturel, Anna Montagnini, Laurent Perrinet*

September 19, 2019

Abstract

Animal behavior must constantly adapt to changes, for example when the statistical properties of the environment change unexpectedly. For an agent that interacts with this volatile setting, it is important to react accurately and as quickly as possible. It has already been shown that when a random sequence of motion ramps of a visual target is biased to one direction (e.g. right or left), human observers adapt to accurately anticipate the expected direction with their eye movements. Here, we prove that this ability extends to a volatile environment where the probability bias could change at random switching times. In addition, we also recorded the explicit direction prediction reported by observers as given by a rating scale. Both results were compared to the estimates of a probabilistic agent that is optimal in relation to the event switching generating model. Compared to the classical leaky integrator model, we found a better match between our probabilistic agent and the behavioral responses, both for the anticipatory eye movements and the explicit task. Furthermore, by titrating the level of preference between exploration and exploitation in the model, we were able to fit each individual experimental data-set with different levels of estimated volatility and derive a common marker for the inter-individual variability of participants. These results prove that in such an unstable environment, human observers can still represent an internal belief about the environmental contingencies, and use this representation both for sensory-motor control and for explicit judgments. This work offers an innovative approach to more generically test the diversity of human cognitive abilities in uncertain and dynamic environments.

Author summary

Understanding how humans adapt to changing environments to make judgments or plan motor responses based on time-varying sensory information is crucial for psychology, neuroscience and artificial intelligence. Current theories for how we deal with the environment's uncertainty most rely on the equilibrium behavior in response to the introduction of some randomness change. Here we show that in the more ecological case where the context switches at random times all along the experiment, an adaptation to this volatility can be performed online. In particular, we show in two behavioral experiments that humans can adapt to such volatility at the early sensorimotor level, through their anticipatory eye movements, but also at a higher cognitive level, through explicit ratings. Our results suggest that humans (and future artificial systems) can use much richer adaptive strategies than previously assumed.

*Institut de Neurosciences de la Timone (UMR 7289), Aix Marseille Univ, CNRS - Marseille, France

1 Motivation

1.1 Volatility of sensory contingencies and the adaptation of cognitive systems

We live in a fundamentally volatile world for which our cognitive system has to constantly adapt. In particular, this volatility may be generated by processes with different time scales. Imagine for instance you are a general practitioner and that you usually report an average number of three persons infected by measles per week. However, this rate is variable and over the past week you observe that the rate increased to ten cases. As such, two alternative interpretations are available: the first possibility is that there is an outbreak of measles and one should then estimate its incidence (i.e. the rate of new cases) since the inferred outbreak's onset, in order to quantify the infection rate specific to this outbreak, but also to update the value of the environmental volatility (as given by the probability of a new outbreak) at a longer time scale. Alternatively, these cases are "unlucky" coincidences that originate from the natural variability of the underlying statistical process which drive patients to the doctor, but which are instances drawn from a stationary random process. In that option, it may be possible to readjust the estimated baseline rate of infection with this new data. This example illustrates one fundamental problem with which our cognitive system is faced: when observing new sensory evidence, *should I stay* and continue to exploit this novel data with respect to my current beliefs about the environment's state or *should I go* and explore a new hypothesis about the random process generating the observations since the detection of a switch in the environment?

By definition, volatility measures the temporal variability of the sufficient parameters of a random variable. Such *meta-analysis* of the environment's statistical properties is an effective strategy at the large scale level of our example, but also at all levels which are behaviorally relevant, such as contextual changes in our everyday life. Inferring near-future states in a dynamic environment, such that one can prepare to act upon them ahead of their occurrence [1] — or at least forming beliefs as precise as possible about a future environmental context — is an ubiquitous challenge for cognitive systems [2]. In the long term, how the human brain dynamically manages this trade-off between exploitation and exploration is essential to the adaptation of the behavior through reinforcement learning [3]. In controlled experimental settings which challenge visual perception or sensorimotor associations, such adaptive processes have been mostly put in evidence by precisely analyzing the participants' behavior in a sequence of experimental trials, typically highlighting sequential effects at the time scale of several seconds to minutes or even hours in the case of the adaptation to a persistent sensorimotor relation.

Indeed, stimulus history of sensory events influences how the current stimulus is perceived [4–8] and acted upon [9–12]. Two qualitatively opposite effects of the stimulus history have been described: negative (adaptation), and positive (priming-like) effects. Adaptation reduces the sensitivity to recurrently presented stimuli, thus yielding to a re-calibrated perceptual experience [13–15]. Examples of negative biases in perceptual discrimination are numerous (see for instance [6, 16]) and show that the visual system tends to favor temporal and spatial stability of the stimulus. On the other hand, priming is a facilitatory effect that enhances the identification of repeated stimuli [17, 18]. In sensorimotor control, the same stimulus presented several times could indeed lead to faster and more accurate responses and, at the same time, lead to critically suboptimal behavior when a presented stimulus is not coherent with the participant's expectations [19, 20]. This process is highly dynamic especially in complex environments where new contingencies can arise at every moment. Interestingly, priming effects at cognitive levels are sometimes paralleled by anticipatory motor

responses which are positively correlated with the repetition of stimulus properties. A well-known example of this behavior are anticipatory smooth eye movements (aSPEM), as we will illustrate in the next section.

Overall, the ability to detect statistical regularities in the event sequence appears as a fundamental ability for the adaptive behavior of living species. Importantly, few studies have addressed the question of whether the estimate of such regularities is explicit, and whether verbal reports of the dynamic statistical estimates would eventually correlate to the measures of behavioral adaptation or priming. Here we aim at investigating this question in the specific case of the processing of a target's motion direction. In addition, we attempt to palliate to the lack of a solid modeling approach to best understand the computation underlying behavioral adaptation to the environment's statistics, and in particular how sequential effects are integrated within a hierarchical statistical framework. As such, Bayesian inference offers an effective methodology to deal with this question. In all generality, Bayesian methods allow to define and quantitatively assess a range of hypotheses about the processing of (possibly noisy) information by some formal agents [21–23]. A key principle in the Bayesian inference approach is to introduce so-called latent variables which formalize how different hypotheses predict synthetic or experimental measurements. Each stated hypothesis is quantitatively formalized by defining a graph of probabilistic dependencies between specific variables using a generative model for the prior knowledge about its structure. In practice, the generative model is parameterized by structural variables (such as weights or non-linear gain functions) such that, knowing incoming measurements, beliefs about latent variables may be represented as probabilities. Then, using the rules of probability calculus one can progressively update beliefs about the latent variables, such that one can finally infer the hidden structure of received inputs [24, 25]. For instance, using Bayes's rule, one can combine the likelihood of observations given the generative model and the prior of these latent variables [26]. Of particular interest for us is the possibility to quantitatively represent in this kind of probabilistic model the predictive and iterative nature of a sequence of events. Indeed, once the belief about latent variables is formed from the sensory input, this belief can be used to update the prior over future beliefs [27]. In such models, the comparisons between expectations and actual data produces constant updates to the estimates of the latent variables but also on the validity of the model. There are numerous examples of Bayesian approaches applied to the study of the adaptation to volatility. For instance, [28] simulated a hierarchical Bayesian model over five previously published datasets [29–33] in the domain of cognitive neuroscience. Their main conclusion was that learning the local transition probabilities was sufficient to explain the large repertoire of experimental effects reported in all these studies. Here we focus on an extension of this approach to the study of motion processing and eye movements.

1.2 Anticipatory Smooth Pursuit Eye Movements (aSPEM)

Humans are able to accurately track a moving object with a combination of saccades and Smooth Pursuit Eye Movements (SPEM, for a review see [34]). These movements allow us to align and stabilize the object on the fovea, thus enabling high-resolution visual processing. This process is delayed by different factors such as axonal transduction, neural processing latencies and the inertia of the oculomotor system [35]. When predictive information is available about target motion, anticipatory SPEM (aSPEM) are efficiently generated before the target's appearance [36–38] thereby reducing visuomotor latency. Moreover, some experiments have demonstrated the existence of prediction-based smooth pursuit during the transient disappearance of a moving target [39–41]. Overall, although the initiation of SPEM is almost always driven by a visual motion signal, it is now clear that smooth pursuit behavior can be

modulated by extra-retinal, predictive information even in the absence of a direct visual stimulation. The anticipatory smooth pursuit behavior is remarkable in different aspects. First, its buildup is relatively fast, such that only a few trials are sufficient to pick up some regularity in the properties of visual motion, such as speed or direction [11, 42, 43]. Second, it is in general an unconscious process of which participants are not aware of. As such, this behavior is potentially a useful marker to study the internal representation of motion expectancy and in particular to analyze how sensorimotor expectancy interacts dynamically with contextual contingencies in shaping oculomotor behavior.

Typically, an aSPEM is observed after a temporal cue and before target motion onset [37, 38, 42]. It is generally assumed that the role of aSPEMs is to minimize as fast as possible the visual impairment due to the amplitude of eye-to-target position and velocity mismatch. Overall, anticipation can potentially reduce the typical sensorimotor delay between target motion onset and foveation. In a previous study [44], we have analyzed how forthcoming motion properties, such as target speed or direction, can be predicted and anticipated with coherently oriented eye movements. It has been observed that the strength of anticipation, as measured by the mean anticipatory eye velocity, increases when the target repeatedly moves in the same direction [42, 45, 46]. We similarly found a graded effect of both the speed and the direction-bias on the strength of aSPEM. In particular, this effect is linearly related to the probability of motion's speed or direction. These results are coherent within previous oculomotor findings by our and also other groups [47]. These results imply that the probability bias over a target's direction is one additional factor beyond other physical and cognitive cues [12, 47, 48] that modulate the common predictive framework driving anticipatory behavior.

1.3 Contributions

The goal of this study is to generalize the adaptive process observed in the aSPEM response in previous studies [44, 47] to more ecological settings and also to broaden its scope by showing that such adaptive processes occur at the conscious level as well. We already mentioned that by manipulating the probability bias for target motion direction, it is possible to modulate the direction and mean velocity of aSPEM. This suggests that probabilistic information may be used to inform the internal representation of motion prediction for the initiation of anticipatory movements. However, it is yet unclear what generative model to use to dynamically manipulate the probability bias and generate an ecologically relevant input sequence of target directions. A possible confound comes from the fact that previous studies have used trial sequences (*blocks*) of fixed lengths, stacked in a sequence of conditions defined by the different probability biases. Indeed, observers may potentially pick up the information on the fixed block's length to predict the occurrence of a switch (a change in probability bias) during the experiment. Second, we observed qualitatively that following a switch, the strength of aSPEM changed gradually, consistently with other adaptation paradigms [49–51]. The estimate of the characteristic temporal parameters for this adaptation mechanism may become particularly challenging in a dynamic context, where the probabilistic contingencies vary in time in an unpredictable way. Finally, whether and how the information processing underlying the buildup of aSPEM and its dynamics is linked to an explicit estimate of probabilities is still largely unknown.

To assess the dynamics of the adaptive processes which compensate for the variability within sensory sequences, one may generate random sequences of Target Directions (TDs) using a dynamic value for the probability bias $p = \Pr(\text{TD is 'right'})$, with a parametric mechanism controlling for the volatility at each trial. In the Hierarchical Gaussian Filter model [52], for instance, volatility is controlled as a non-linear transformation of a random walk (modeled itself by a Brownian motion with a given

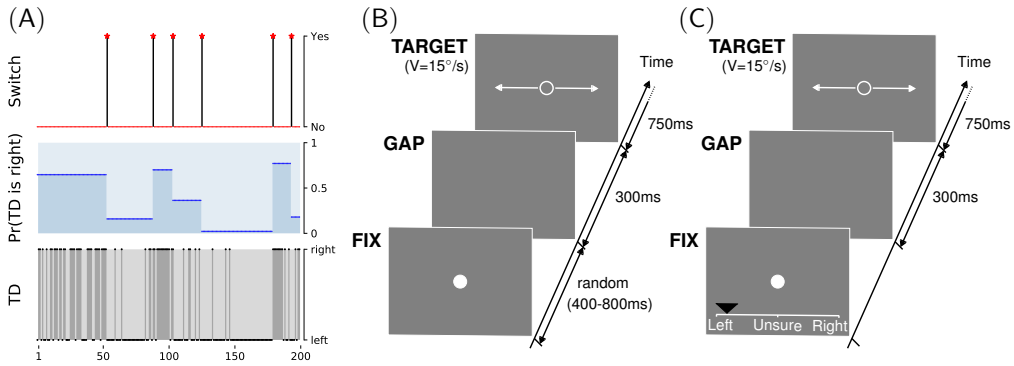

Fig 1. Smooth pursuit eye movements and explicit direction predictions in a volatile switching environment *(A)* We tested the capacity of human participants to adapt to a volatile environment by using a simple, 3-layered generative model of fluctuations in target directions (TD) that we call the Binary Switching Model (BSM). This TD binary variable is chosen using a Bernoulli trial of a given probability bias. This probability bias is constant for as many trials until a switch is generated. At a switch, the bias is chosen at random from a given prior. Switches are generated in the third layer as binary events drawn from a Bernoulli trial with a given hazard rate (defined here as 1/40 per trial). *(B)* The eye-movements task was an adapted version of a task developed by [44]. Each one of 600 trials consisted of sequentially: a fixation dot (of random duration between 400 and 800 ms), a blank screen (of fixed duration of 300 ms) and a moving ring-shaped target (with 15 $°/s$ velocity) which the observers were instructed to follow. The direction of the target (right or left) was drawn pseudo-randomly according to the generative model defined above. *(C)* In order to titrate the adaptation to the environmental volatility of target direction at the conscious level, we invited each observer to perform on a different day a new variant of the direction-biased experiment, where we asked participants to predict, before each trial, their estimate of the forthcoming direction of the target. As shown in this sample screenshot, this was performed by moving a mouse cursor (black triangle) on a continuous rating scale between "sure left", to "unsure" and finally "sure right".

diffusion coefficient). Ultimately, this hierarchical model allows to generate a sequence of binary choices where the variability fluctuates along a given trajectory. Such a forward probabilistic model is invertible using some simplifying assumptions and allows to extract a time-varying inference of the agent's belief about volatility [53]. Herein, to analyze the effect of history length in all generality, we extended the protocol of [44] such that the probability bias is still fixed within blocks but that these blocks have variable lengths, that is, by introducing switches occurring at random times. Therefore, similarly to [54], we will use a model where the bias p in target direction varies according to a piecewise-constant function. In addition, in our previous study the range of possible biases was finite. In the present work, we extended the paradigm by drawing p as a continuous random variable within the whole range of possible probability biases (that is, the segment $[0, 1]$). As a summary, we first draw random events (that we denote as "switches") with a given mean frequency and which controls the strength of the volatility. Second, the value p of the bias only changes at the moment of a switch, independently of the previous bias' value and is stationary between two switches, forming what we call an "epoch". Third, target direction is drawn as a Bernoulli trial using the current value of p. Such a hierarchical structure is presented in Figure 1-A, where we show the realization of the target's directions sequence, the trajectory of the underlying probability bias (hidden to the observer), and the occurrences of switches.

Mathematically, this can be considered as a three-layered hierarchical model defining the evolution of the model at each trial t as the vector (x_2^t, x_1^t, x_0^t). At the topmost layer, the occurrence $x_2^t \in \{0, 1\}$ of a switch (1 for true, 0 for false) is drawn from a Bernoulli trial $\mathcal{B}$ parameterized by its frequency h, or *hazard rate*. The value of $\tau = \frac{1}{h}$ thus gives the average duration (in number of trials) between the occurrence of two switches. In the middle layer, the probability bias p of target direction is a random variable that we define as $x_1^t \in [0, 1]$. It is chosen at random from a prior distribution $\mathcal{P}$ at the moment of a switch, and else it is constant until the next occurrence of a switch. The prior distribution $\mathcal{P}$ can be for instance the uniform distribution $\mathcal{U}$ on $[0, 1]$ or Jeffrey's prior $\mathcal{J}$ (see Appendix 8.3). Finally, a target moves either to the left or to the right, and we denote this variable (target direction, TD) as $x_0^t \in \{0, 1\}$. This direction is drawn from a Bernoulli trial parameterized by the direction bias $p = x_1^t$. In summary, this is described according to the following equations:

$$\begin{cases} \text{Occurrence of a switch: } x_2^t \propto \mathcal{B}(1/\tau) \\ \text{Dynamics of probabilistic bias } p = x_1^t\text{: } \begin{cases} \text{if} \quad x_2^t = 0 \quad \text{then} \quad x_1^t = x_1^{t-1} \\ \text{else} \quad x_1^t \propto \mathcal{P} \end{cases} \\ \text{Sequence of directions: } x_0^t \propto \mathcal{B}(x_1^t) \end{cases} \tag{1}$$

In practice, we generated a sequence of 600 trials, and there is by construction a switch at $t = 0$ (that is, $x_2^0 = 1$). In addition, we imposed in our sequence that a switch occurs after trial numbers 200 and 400, in order to be able to compare adaptation properties across different chunks of the trials sequence. With such a three-layered structure, the model generates the randomized occurrence of switches, itself generating epochs with constant direction probability and finally the random sequence of Target Direction (TD) occurrences at each trial. To sum up, the system of three equations defined in Equation 1 defines the Binary Switching Model (BSM) which we used for the generation of experimental sequences presented to human participants in the experiments. We will use that generative model as the basis of an ideal observer model inverting that model to predict probability biases from the observations (TDs) and which we will test as a model for the adaptation of human behavior.

This paper is organized in five parts. After this introduction where we presented the motivation for this study, the next section (Section 2) will present an inversion of the BSM forward probabilistic model, coined the Binary Bayesian Change Point (BBCP)

model. To our knowledge, such algorithm was not yet available, and we will here provide with an exact analytical solution by extending previous results from [55] to the case of binary data as in the BSM presented above (see Equation 1). In addition, the proposed algorithm is biologically realistic as it uses simple computations and is *online*, that is, that all computations on the sequence may be done using solely a set of variables available at the present trial, compactly representing all the sequence history seen in previous trials. We will also provide a computational implementation and a quantitative evaluation of this algorithm. Then, we will present in Section 3 the analysis of experimental evidence to validate the generalization of previous results with this novel protocol. In one session, participants were asked to estimate "how much they are confident that the target will move to the right or left in the next trial" and to adjust the cursor's position on the screen accordingly (see Figure 1-C). In the other experimental session on a different day, we showed the same sequence of target directions and recorded participants' eye movements (see Figure 1-B). Indeed, in order to understand the nature of the representation of motion regularities underlying this adaptive behavior, it is crucial to collect both the recording of eye movements and the verbal explicit judgments about expectations on motion direction. Another novelty of our approach is to use that agent as a regressor which will allow us to match experimental results with the BBCP and to compare its predictive power compared to classical models such as the leaky integrator model. Hence, we will show that behavioral results match well with the BBCP model. In Section 4, we will synthesize these results by inferring the volatility parameters inherent to the models by best-fitting it to each each individual participant. This will allow the analysis of inter-individual behavioral responses for each session. In particular, we will test if one could predict observers' prior (preferred) volatility, that is, a measure of the dynamic compromise between exploration ("should I go?") and exploitation ("should I stay?") across the two different sessions challenging predictive adaptive processes at the unconscious and conscious levels. Finally, we will summarize and conclude this study and offer some perspectives for future work in Section 5.

2 Results: Binary Bayesian Change Point (BBCP) detection model

As we saw above, Bayesian methods provide a powerful framework for studying human behavior and adaptive processes in particular. For instance, [52] first defined a multi-layered generative model for sequences of input stimuli. By inverting this stochastic forward process, they could extract relevant descriptors at the different levels of the model and fit these parameters with the recorded behavior. Here, we use a similar approach, focusing specifically on the BSM generative model, as defined in Equation 1. To begin, we define a first ideal observer as a control, the *leaky integrator* (or *forgetful agent*), which has an exponentially-decaying memory for the events that occurred in the past trials. This agent can equivalently be described as one which assumes that volatility is stationary with a fixed characteristic frequency of switches. Then, we will extend this model to an agent which assumes the existence of (randomly occurring) switches, that is, that the value of the probabilistic bias may change at specific (yet randomly drawn) trials, as defined by the forward probabilistic model in Equation 1.

2.1 Forgetful agent model (Leaky integrator)

The leaky integrator ideal observer represents a classical, widespread and realistic model of how trial-history shapes adaptive processes in human behavior. It is also well adapted to model motion expectation in the direction-biased experiment which leads to

anticipatory SPEMs. In this model, given the sequence of observations x_0^t from trial 0 to t, the expectation $p = \hat{x_1}^{t+1}$ of the probability for the next trial direction can be modeled by making a simple heuristic: This probability for an event is the weighted average of the previously estimated probability, $\hat{x_1}^t$, with the new information x_0^t, where the weight corresponds to a leak term (or discount) by a factor $(1-h)$, with $h \in [0,1]$ [56]. At trial t, this model can be expressed with the following equation:

$$\hat{x_1}^{t+1} = (1-h) \cdot \hat{x_1}^t + h \cdot x_0^t \tag{2}$$

where $\hat{x_1}^{t=0}$ is equal to some prior value (0.5 in the unbiased case), corresponding to the best guess at $t = 0$ (prior to the observation of any data).

In other words, the estimated probability $\hat{x_1}^{t+1}$ is computed from the integration of previous instances with a progressive discount of past information. The value of the scalar h represents a compromise between responding rapidly to changes in the environment ($h \approx 1$) and not prematurely discarding information still of value for slowly changing contexts ($h \approx 0$). As such, we will call this scalar the hazard rate. Similarly, one can define $\tau = 1/h$ as a characteristic time (in units of number of trials) for the integration of information. Looking more closely at this expression, the "forgetful agent" computed in Equation 2 consists of an exponentially-weighted moving average (see Appendix 8.1). It may thus be equivalently written in the form of a time-weighted average:

$$\hat{x_1}^{t+1} = (1-h)^{t+1} \cdot \hat{x_1}^{t=0} + h \cdot \sum_{0 \leq i \leq t} (1-h)^i \cdot x_0^{t-i} \tag{3}$$

The first term corresponds to the discounted effect of the prior value before any observation and it tends to 0 when t increases. More importantly, as $1-h < 1$, the second term corresponds to the *leaky* integration of novel observations. Inversely, let us now assume that the true probability bias for direction changes randomly with a mean rate of once every τ trials. As a consequence, the probability that the bias does not change is $Pr(x_2^t = 0) = 1-h$ at each trial. Assuming independence of these occurrences, the estimated probability $p = \hat{x_1}^{t+1}$ is thus proportional to the sum of the past observations weighted by the belief that the bias has not changed during i trials in the past, that is, exactly as defined by the second term of the right-hand side in Equation 3. This shows that assuming that changes occur at a constant rate ($\hat{x_2}^t = h$) but ignoring the variability in the temporal occurrence of the switch, the optimal solution to this inference problem is the ideal observer defined in Equation 3, which finds an online recursive solution in Equation 2. We therefore proved here that the heuristic derived from [56] is an ideal inversion of the two-layered generative model which assumes a constant hazard rate for the probability bias.

The correspondence that we proved between the weighted moving average heuristic and the forgetful agent model as an ideal solution to that generative model leads us to several interim conclusions. First, the time series of inferred $\hat{x_1}^{t+1}$ values can serve as a regressor for behavioral data to test whether human observers follow a similar strategy. In particular, the free parameter h may be fitted to variations of the behavioral data across the sequence, which itself is assumed to depend on the agents' belief in the weight decay. Now, since we have defined a first generative model and the corresponding ideal observer (the forgetful agent), we next define a more complex model, in order to overcome some of the limits of the leaky integrator. Indeed, a first criticism could be that this model is too rigid and does not sufficiently account for the dynamics of contextual changes [57] as the weight decay corresponds to assume *a priori* a constant precision in the data sequence, contrary to more elaborate Bayesian models [58]. It seems plausible that the memory size (or history length) used by the brain to infer any event probability can vary, and that this variation could be related to the environmental volatility inferred from past data. The model presented in Equation 3

uses a constant weight (decaying with the distance to the current trial) for all trials, while the actual precision of each trial can be potentially evaluated and used for precision-weighted estimation of the probability bias. To address this hypothesis, our next model is inspired by the Bayesian Change-point detection model [55] of an ideal agent inferring both the trajectory in time of the probability bias (x_1^t) but also of the probability $Pr(x_2^t = 1)$ of the occurrence of switches.

2.2 Binary Bayesian Change Point (BBCP) detection model

There is a crucial difference between the forgetful agent presented above and an ideal agent which would invert the Binary Switching Model (BSM, see Equation 1). Indeed, at any trial during the experiment, the agent may infer beliefs about the probability of the volatility x_2^t which itself is driving the trajectory of the probability bias x_1^t. Knowing that the latter is piece-wise constant, an agent may have a belief over the number of trials since the last switch. This number, that is called the *run-length* r^t, is useful in two manners. First, it allows the agent to restrict the prediction $\hat{x_1}^{t+1}$ of x_1^{t+1} only based on those samples produced since the last switch, from $t - r^t$ until t. Indeed, the samples x_0^t which occurred before the last switch were drawn independently from the present true value x_1^t and thus cannot help estimating the latter. Second, it is known that for this estimate, the precision (the inverse of variance) on the estimate $\hat{x_1}^{t+1}$ grows linearly with the number of samples: The longer the run-length, the sharper the corresponding (probabilistic) belief. We have designed an agent inverting the BSM by extending the Bayesian Change-Point (BCP) detection model [55]. The latter model defines the agent as an inversion of a switching generative model for which the observed data (input) is Gaussian. We present here an exact solution for the case of the BSM, where the input is binary.

In order to define in all generality the switch detection model, we will initially describe the fundamental steps leading to its construction, while providing the full algorithmic details in Appendix 8.3. The goal of predictive processing is to infer the probability $Pr(x_0^{t+1}|x_0^{0:t})$ of the next datum knowing what has been observed until trial t (that we denote by $x_0^{0:t} = \{x_0^0, \ldots, x_0^t\}$), as well the agent's prior knowledge that data is the output of a given (stochastic) generative model (here, the BSM). To derive a Bayesian predictive model, we introduce the run-length as a latent variable which gives to the agent the possibility to represent different parallel hypotheses about the input. We therefore draw a computational graph (see Figure 2-A) where, at any trial, an hypothesis is formed on as many "nodes" than there are run-lengths (and limited for instance by the total number of trials). As a readout, we can use this knowledge of the predictive probability conditioned on the run-length, such that one can compute the marginal predictive distribution:

$$Pr(x_0^{t+1}|x_0^{0:t}) = \sum_{r^t \geq 0} Pr(x_0^{t+1}|r^t, x_0^{0:t}) \cdot \beta_t^{(r)} \tag{4}$$

where $Pr(x_0^{t+1}|r^t, x_0^{0:t})$ is the Bernoulli trial modeling the probability of a future datum x_0^{t+1} conditioned on the run-length and $\beta_t^{(r)} = Pr(r^t|x_0^{0:t})$ is the probability for each possible run-length given the observed data. Note that $\beta_t^{(r)}$ is scaled such that $\sum_{r \geq 0} \beta_t^{(r)} = 1$. Indeed, we know that, at any trial, there is a single true value for this variable r^t and that $\beta_t^{(r)}$ thus represents the agent's inferred probability distribution over the run-length r.

With these premises, we define the BBCP as a prediction / update cycle which connects nodes from the previous trial to that at the current trial. Indeed, we will *predict* the probability $\beta_t^{(r)}$ at each node, knowing either an initial prior, or its value on

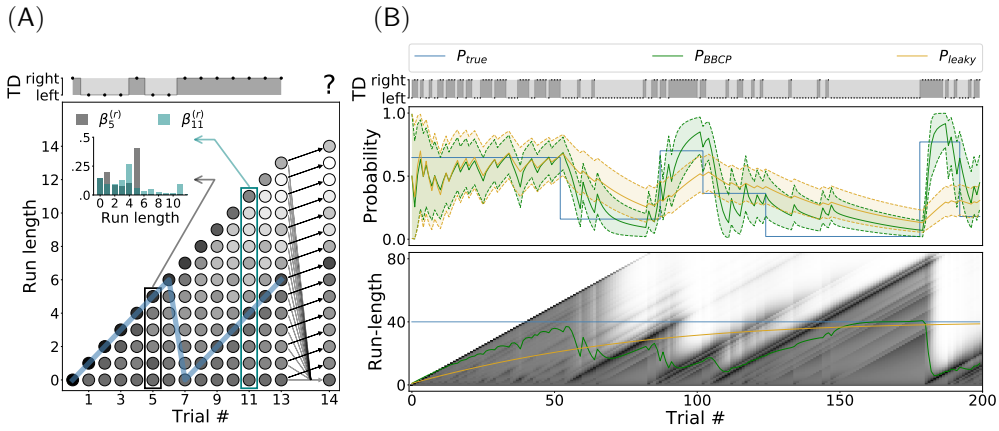

Fig 2. Binary Bayesian Change Point (BBCP) detection model. *(A)* This plot shows a synthesized sequence of 13 events, either a leftward or rightward movement of the target (TD). Run-length estimates are expressed as hypotheses about the length of a sub-block over which the probability bias was constant, that is, the number of trials since the last switch. Here, the true probability bias switched from a value of .5 to .9 at trial 7, as can be seen by the trajectory of the true run-length (blue line). The BBCP model tries to capture the occurrences of a switch by inferring the probability of different possible run lengths. At any new datum (trial), this defines a Hidden Markov Model as a graph (treillis), where edges indicate that a message is being passed to update each node's probability (as represented by arrows from trial 13 to 14). Black lines denote a progression of the run length at the next step (no switch), while gray lines stand for the possibility that a switch happened: In this case the run length would fall back to zero. The probability for each node is represented by the grey scale (darker grey colors denote higher probability) and the distribution is shown in the inset for two representative trials: 5 and 11. Overall, this graph shows how the model integrates information to accurately identify a switch and produce a prediction for the next trial (e.g. for $t = 14$). *(B)* On a longer sequence of 200 trials, representative of a sub-block of our experimental sequence (see Figure 1-A), we show the actual events which are observed by the agent (TD), along with the (hidden) dynamics of the true probability bias P_{true} (blue line), the value inferred by a leaky integrator (P_{leaky}, orange line) and the results of the BBCP model in estimating the probability bias P_{BBCP} (green line), along with .05 and .95 quantiles (shaded area). This shows that for the BBCP model, the accuracy of the estimated value of the probability bias is higher than for the leaky integrator. Below we show the belief (as grayscales) for the different possible run lengths. The green and orange line correspond to the mean run-length which is inferred, respectively, by the BBCP and leaky models: Note that in the BBCP, while it takes some trials to detect switches, they are in general correctly identified (transitions between diagonal lines) and that integration is thus faster than for the leaky integrator, as illustrated by the inferred value of the probability bias.

a previous trial. In particular, at the occurrence of the first trial, we know for certain that there is a switch and initial beliefs are thus set to the values $\beta_0^{(0)} = Pr(r^t = 0) = 1$ and $\forall r > 0$, $\beta_0^{(r)} = Pr(r^0 = r) = 0$. Then, at any trial $t > 0$, as we observe a new datum x_0^t, we use a knowledge of $\beta_{t-1}^{(r)}$ at trial $t-1$, the likelihood $\pi_t^{(r)} = Pr(x_0^t | r^{t-1}, x_0^{0:t-1})$ and the transition probabilities defined by the generative model to predict the beliefs over all nodes:

$$\beta_t^{(r)} \propto \sum_{r^{t-1} \geq 0} \beta_{t-1}^{(r)} \cdot Pr(r^t | r^{t-1}) \cdot \pi_t^{(r)} \tag{5}$$

In the computational graph, Equation 5 corresponds to a message passing from the nodes at time $t-1$ to that at time t. We will now detail how to compute the transition probabilities and the likelihood.

First, knowing that the data is generated by a switching model such as the BSM (see Equation 1), the run-length is either null at the moment of a switch, or its length (in number of trials) is incremented by 1 if no switch occurred:

$$\begin{cases} \text{if} \quad x_2^t = 1, \quad r^t = 0 \\ \text{if} \quad x_2^t = 0, \quad r^t = r^{t-1} + 1 \end{cases} \tag{6}$$

This may be illustrated by a graph in which information will be represented at the different nodes for each trial t. This defines the transition matrix $Pr(r^t | r^{t-1})$ as a partition in two exclusive possibilities: Either there was a switch or not. It allows us to compute the *growth probability* for each run-length. On the one hand, the belief of an increment of the run-length at the next trial is:

$$\beta_t^{(r+1)} = \frac{1}{B} \cdot \beta_{t-1}^{(r)} \cdot \pi_t^{(r)} \cdot (1-h) \tag{7}$$

where h is the scalar defining the hazard rate. On the other hand, it also allows to express the change-point probability as:

$$\beta_t^{(0)} = \frac{1}{B} \cdot \sum_{r \geq 0} \beta_{t-1}^{(r)} \cdot \pi_t^{(r)} \cdot h \tag{8}$$

with B such that $\sum_{r \geq 0} \beta_t^{(r)} = 1$. Note that $\beta_t^{(0)} = h$ and thus $B = \sum_{r \geq 0} \beta_{t-1}^{(r)} \cdot \pi_t^{(r)}$. Knowing this probability strength and the previous value of the prediction, we can therefore make a prediction for our belief of the probability bias at the next trial $t+1$, prior to the observation of a new datum x_0^{t+1} and resume the prediction / update cycle (see Equations 4, 7 and 8).

Integrated in our cycle, we *update* beliefs on all nodes by computing the likelihood $\pi_t^{(r)}$ of the current datum x_0^t knowing the current belief at each node, that is, based on observations from trials 0 to $t-1$. A major algorithmic difference with the BCP model [55], is that here the observed data is a Bernoulli trial and not a Gaussian random variable. The random variable x_1^t is the probability bias used to generate the sequence of events x_0^t. We will infer it for all different hypotheses on r^t, that is, knowing there was a sequence of r^t Bernoulli trials with a fixed probability bias in that epoch. Such an hypothesis will allow us to compute the distribution $Pr(x_0^{t+1} | r^t, x_0^{0:t})$ by a simple parameterization. Mathematically, a belief on the random variable x_1^t is represented by the conjugate probability distribution of the binomial distribution, that is, by the beta-distribution $B(x_1^t; \mu_t^{(r)}, \nu_t^{(r)})$. It is parameterized here by its sufficient

statistics, the mean $\mu_t^{(r)}$ and sample size $\nu_t^{(r)}$ (see Appendix 8.2 for our choice of parameterization). First, at the occurrence of a switch (for the node $r^t = 0$) beliefs are set to prior values (before observing any datum) $\mu_t^{(0)} = \mu_{prior}$ and $\nu_t^{(0)} = \nu_{prior}$. By recurrence one can show that at any trial $t > 0$, the sufficient statistics $(\mu_t^{(r)}, \nu_t^{(r)})$ can be updated from the previous trial following:

$$\nu_t^{(r+1)} = \nu_{t-1}^{(r)} + 1 \tag{9}$$

As a consequence, $\forall r, t; \nu_t^{(r)}$ is the sample size corrected by the initial condition. $\nu_t^{(r)} = r + \nu_{prior}$. For the mean, the series defined by $\mu_t^{(r+1)}$ is the average at trial t over the $r+1$ last samples, which can also be written in a recursive fashion:

$$\mu_t^{(r+1)} = \frac{1}{\nu_t^{(r+1)}} \cdot (\nu_{t-1}^{(r)} \cdot \mu_{t-1}^{(r)} + x_0^t) \tag{10}$$

This updates for each node the sufficient statistics of the probability density function at the current trial. We can now detail the computation of the likelihood of the current datum x_0^t with respect to the current beliefs : $\pi_t^{(r)} = Pr(x_0^t | \mu_{t-1}^{(r)}, \nu_{t-1}^{(r)})$. This scalar is returned by the binary function $\mathcal{L}(r|o)$ which evaluates at each node r the likelihood of the parameters of each node whenever we observe a counterfactual alternative outcome $o = 1$ or $o = 0$ knowing a mean bias $p = \mu_{t-1}^{(r)}$ and a sample size $r = \nu_{t-1}^{(r)}$. For each outcome, the likelihood of observing an occurrence of o, is the probability of a binomial random variable knowing an updated probability bias of $\frac{p \cdot r + o}{r+1}$, a number $p \cdot r + o$ of trials going to the right and a number $(1-p) \cdot r + 1 - o$ of trials to the left. After some algebra, this defines the likelihood as :

$$\mathcal{L}(r|o) = \frac{1}{Z} \cdot (p \cdot r + o)^{p \cdot r + o} \cdot ((1-p) \cdot r + 1 - o)^{(1-p) \cdot r + 1 - o} \tag{11}$$

with Z such that $\mathcal{L}(r|o=1) + \mathcal{L}(r|o=0) = 1$. The full derivation of this function is detailed in Appendix 8.4. This provides us with the likelihood function and finally the scalar value $\pi_t^{(r)} = \mathcal{L}(r|x_0^t)$.

Finally, the agent infers at each trial the belief and parameters at each node and uses the marginal predictive probability (see Equation 4) as a readout. This probability bias is best estimated by its expected value $\hat{x_1}^{t+1} = Pr(x_0^{t+1} | x_0^{0:t})$ as it is marginalized over all run-lengths:

$$\hat{x_1}^{t+1} = \sum_{r \geq 0} \mu_t^{(r)} \cdot \beta_t^{(r)} \tag{12}$$

Interestingly, it can be proven that if, instead of updating beliefs with Equations 7 and 8, we set nodes' beliefs to the constant vector $\beta_t^{(r)} = h \cdot (1-h)^r$, then the marginal probability is equal to that obtained with the leaky integrator (see Equation 2). This highlights again that, contrary to the leaky integrator, the BBCP model uses a dynamical model for the estimation of the volatility. Still, as for the latter, there is only one parameter $h = \frac{1}{\tau}$ which informs the BBCP model that the probability bias switches *on average* every τ trials. Moreover, note that the resulting operations (see Equations 4, 7, 8, 11 and 12) which constitute the BBCP algorithm can be implemented *online*, that is, only the state at trial t and the new datum x_0^t are sufficient to predict all probabilities for the next trial. Finally, this prediction/update cycle applied to the BSM and using Equation 1 constitutes the Binary Bayesian Change Point (BBCP) detection model.

2.3 Quantitative analysis of the Binary Bayesian Change Point detection algorithm

We have implemented the BBCP algorithm using a set of Python scripts. This implementation provides also some control scripts to test the behavior of the algorithm with synthetic data. Indeed, this allows to qualitatively and quantitatively assess this ideal observer model against a ground truth before applying it on the trial sequence that was used for the experiments and ultimately comparing it to the human behavior. Figure 2-A shows a graph-based representation of the BBCP estimate of the run-length for one instance of a short sequence (14 trials) of simulated data x_0^t of leftward and rightward trials, with a switch in the probability bias of moving rightward occurring at trial 7 (see figure caption for a detailed explanation). Figure 2-B, illustrates the predicted probability $\hat{x_1}^t$, as well as the corresponding uncertainty (the shaded areas correspond to .05 and .95 quantiles) when we applied respectively the BBCP (green curve) and the forgetful agent (orange curve) model to a longer sequence of 200 trials, characteristic of our behavioral experiments. In the bottom panel, we show the dynamical evolution of the belief on the latent variable (run length), corresponding to the same sequence of 200 trials. The BBCP model achieves a correct detection of the switches after a short delay of a few trials.

Two main observations are noteworthy. First, after each detected switch, beliefs align along a linear ridge, as our model best estimate of the current run-length is steadily incremented by 1 at each trial until a new switch, and the probability $\hat{x_1}^t$ is estimated by integrating sensory evidence in this epoch (it 'stays'). Then, we observe that shortly after a switch (hidden to the agent), the belief diffuses until the relative probability of a continuously increasing run-length is lower that that assigned to a smaller run-length: There is a transition to a new state (the model 'goes'). Such adaptation is similar to the slow / fast heuristic model proposed in other studies [59]. Second, we can use this information to readout the most likely probability bias and use it as a regressor for the behavioral data. Note that the leaky integrator model is implemented by the agent assuming a fixed run-length profile (see orange line in Figure 2-B), allowing for a simple comparison of the BBCP model with the leaky integrator. Again, we see that a fixed length model gives qualitatively a similar output but with two disadvantages compared to the BBCP model, namely that there is a stronger inertia in the dynamics of the model estimates and that there is no improvement in the precision of the estimates after a switch. In contrast, after a correct switch detection in the BBCP model, the value of the inferred probability converges rapidly to the true probability as the number of observations steadily increases after a switch.

In order to quantitatively evaluate the algorithm and following a similar strategy as [60], we computed an overall cost $\mathcal{C}$ as the negative log-likelihood (in bits) of the estimated probability bias, knowing the true probability and averaged over all T trials:

$$\begin{cases} \mathcal{C} = \frac{1}{T}\sum_t \mathcal{C}(x_1^t, \hat{x_1}^t) \text{ with } \mathcal{C}(x_1^t, \hat{x_1}^t) = H(x_1^t, \hat{x_1}^t) - H(x_1^t, x_1^t) \\ \text{where } H(x_1^t, \hat{x_1}^t) = -x_1{}^t \log_2(\hat{x_1}^t) - (1 - x_1{}^t)\log_2(1 - \hat{x_1}^t) \end{cases} \tag{13}$$

The measure $\mathcal{C}(x_1^t, \hat{x_1}^t)$ explicitly corresponds to the average score of our model, as the Kullback-Leibler distance of $\hat{x_1}^t$ compared to the hidden true probability bias x_1^t. We have tested 100 blocks of 2000 trials for each read-out. In general, we found that the inference is better for the BBCP algorithm ($\mathcal{C} = 0.171 \pm 0.030$) than for the leaky integrator ($\mathcal{C} = 0.522 \pm 0.128$), confirming that it provides overall a better description of the data. Note that the only free parameter of this model is the hazard rate h assumed by the agent (as in the fixed-length agent). Although more generic solutions exist [61–63], we decided as a first step to keep this parameter fixed for our agent, and evaluate how well it matches to the experimental outcomes at the different scales of the

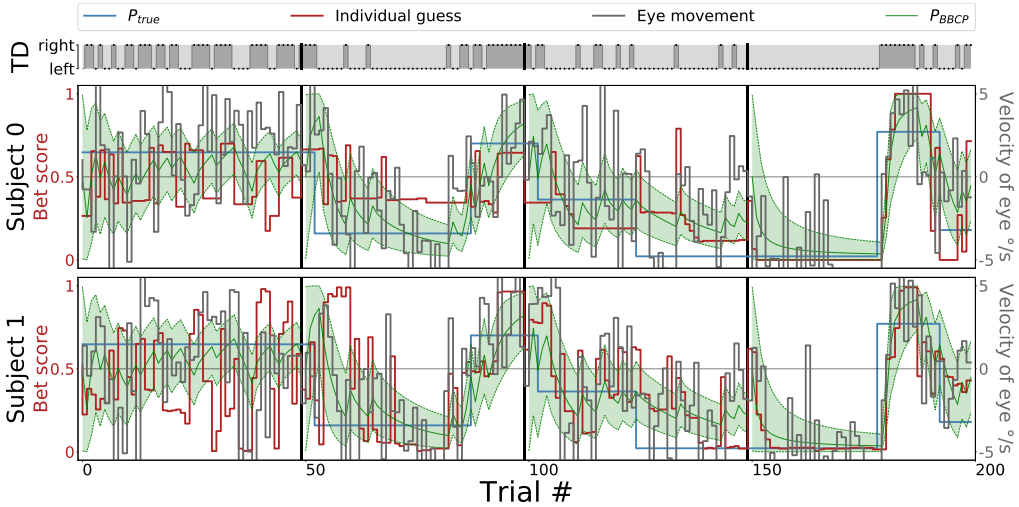

Fig 3. Raw behavioral results, qualitative overview. The top row represents the sequence of target directions (TD) that were presented to observers in one sub-block of 200 trials, as generated by the binary switching model (see Figure 1-A). Bottom two rows show the raw behavioral results for two representative observers: The recorded aSPEM strength as measured by the horizontal eye velocity estimated right before the onset of the visually-driven SPEM (dark gray line); and the explicit ratings about the expected target direction (or *bet scores*, red line). We also show the evolution of the value of the probability bias P_{true} (blue line) which is hidden to observers and used to generate the TD sequence above. We have overlaid the results of the BBCP model (see Figure 2-B, green line). This shows qualitatively a good match between the experimental evidence and the model. Note that short pauses occurred every 50 trials (as denoted by vertical black lines, see main text), and we added the assumption in the model that there was a switch at each pause. This is reflected by the reset of the green curve close to the 0.5 level and the increase of the uncertainty after each pause.

protocol: averaged over all observers, for each individual observer or independently in all individual sub-blocks. In a second step, by testing different values of h assumed by the agent but for a fixed hazard rate $h = 1/40$ in the BSM, we found that the distance given by Equation 13 is minimal for the true hazard rate used to generate the data. In other words, this analysis shows that the agent's inference is best for a hazard rate equal to that implemented in the generative model and which is actually hidden to the BBCP agent. This property will be important in a following section to estimate the hazard rate implicitly assumed by an individual participant on the basis of the set of responses given to the sequence of stimuli (see Section 4). As a summary, for each trial of any given sequence, we obtain an estimate of the probability bias assumed by the ideal observer and which we may use as a regressor. We will now present the analysis of this model's match to our experimental measures of anticipatory eye movements and explicit guesses about target motion direction.

3 Results: Anticipatory eye movements and explicit ratings

We used the BSM model to generate the (pseudo-)random sequence of the dot's directions (the alternation of leftward/rightward trials) as the sequence of observations that were used in both sessions (see Figure 3). In one session, we recorded the

participants' eye movements and we show the anticipatory smooth pursuit velocity for two representative participants (out of 12 participants), throughout a sub-block of 200 trials of the experimental sequence. Note that these participants were chosen as those whose fitting score was nearest to the median score in the quantitative analysis that will be illustrated below in Section 4. In the top panel of Figure 3 we show the actual sequence of binary choices (TD, leftward or rightward) of the Bernoulli trials, whereas in the bottom panels, we compare for each two participants the evolution of the recorded aSPEM (grey line) with the true value of the hidden probability bias x_1 (step-like blue curve), and the value inferred using the BBCP model (green line), along with the .05 to .95 quantile range (green shaded area). Comparing the raw aSPEM results with the BBCP agent predictions, it appears qualitatively that both traces evolve in good agreement. First, one can observe a trend in the polarity of aSPEM velocity to be negative for probability bias values below .5 and positive for values above .5. Moreover, both curves (aSPEM and model) unveil similar delays in detecting and taking into account a switch of the probability bias (while being hidden to the observers), reflecting the time (in the order of a few trials) taken to integrate enough information to build up the estimation of a novel expectation about the probability bias value parameterizing the Bernoulli trial. In general, results are more variable when the bias is weak ($p \approx .5$) than when it is strong (close to zero or one), consistent with the well-known dependence of the variance of a Bernoulli trial upon the probabilistic bias ($\mathrm{Var}(p) = p \cdot (1-p)$). In addition, the precision (i.e. the inverse of the variance) of the inferred probability bias $\hat{x_1}$ seems to increase in longer epochs (inter-switch blocks) as information is integrated over more trials. As a result, the inferred probability as a function of time seems qualitatively to constitute a reliable regressor for predicting the strength of aSPEM.

In addition, the explicit ratings for the next trial's expected motion direction (or *bet scores*, red curve in Figure 3) provided in the other experimental session seem to qualitatively follow the same trend. Indeed, similarly to the strength of aSPEM, we qualitatively compare in Figure 3 the trace of the bet scores with the inferred probability bias $\hat{x_1}$. As with aSPEM, the series of the participants' bias guesses exhibits a positive correlation with the true probability bias: The next outcome of x_0^t will in general be correctly inferred, as compared to a random choice, as reported previously [64]. Moreover, we observe again that a stronger probability bias leads to a lower variability in the bet scores, compared to bias values close to 0.5. Again, a (hidden) switch in the value of the bias is most of the time correctly identified after only a few trials. Finally, note that at every pause (black vertical bar in Figure 3), participants tended to favor unbiased guesses, closer to 0.5 than at the end of a sub-block of trials. We can speculate that this phenomenon could correspond to a spontaneous resetting mechanism of the internal belief on the probability bias and indeed we can introduce such an assumption in the model, as a reset of the internal belief after each pause. To conclude, the experiment performed in this session shows that the probability bias values that are explicitly estimated by participants are qualitatively similar to the implicit (and largely unconscious) ones which supposedly underlie the generation of anticipatory aSPEM with variable strength.

Quantitatively, we now compare the experimental results with the value of the probability bias $\hat{x_1}$ computed by the BBCP algorithm. Compiling results from all participants, we have plotted in Figure 4 the aSPEM strength (panel A) and the bet scores (panel B) as a function of the BBCP-inferred probability bias (we remind here that the true value of the probability bias was coded at the second layer of the BSM generative model and is hidden both to the agents and to the human observers). All trials from all participants were pooled together and we show this joint data as an error bar plot showing the median along with the .25 and .75 quantiles as computed for 5 equal partitions of the $[0, 1]$ probability segment. As a comparison, the same method

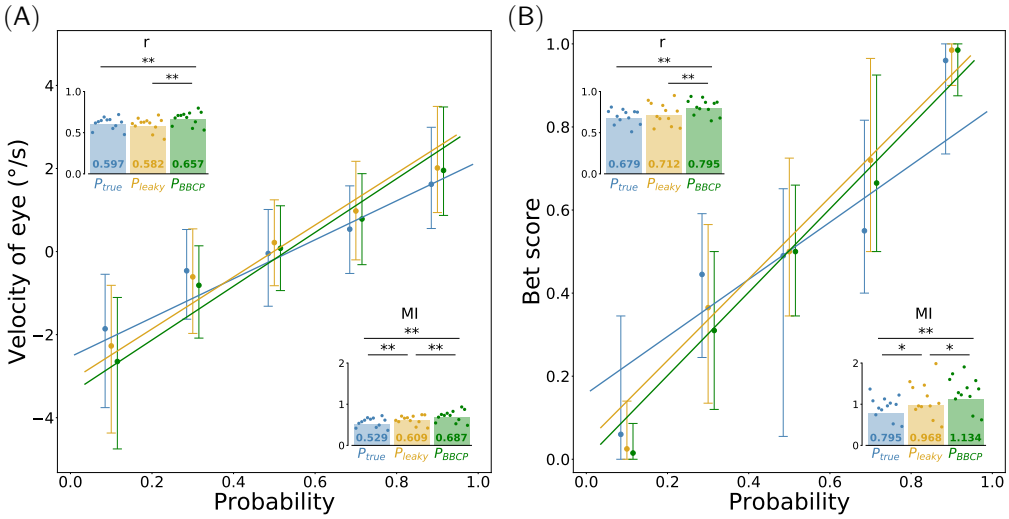

Fig 4. Behavioral results, quantitative analysis across participants. For all participants and for all trials, we collected an estimate of the strength of aSPEM and a bet score value. We analyze the relation between these experimental data with the corresponding prediction P_{BBCP} of the probability bias as inferred by the BBCP model. We display these functional relations using an error-bar plot showing the median with .25 and .75 quantiles over 5 equal partitions of the $[0, 1]$ probability segment. The green regression line illustrates the relationship between the BBCP regressor in abscissa and in ordinate *(A)* the strength of aSPEM and *(B)* the bet score, respectively. As a comparison, we have plotted in blue and orange colors the regression lines with respectively the true probability ($P_{\mathrm{true}} = x_1^t$) and the probability bias estimates P_{leaky} obtained with a leaky integrator. Insets summarize the quantitative measure of this match by computing the Pearson correlation coefficient r and the mutual information (MI) over the whole data set. Dots correspond to these measures for each individual observer. This shows quantitatively that for both experimental measures there is a strong statistical dependency between the behavioral results and the prediction of the BBCP model, but also that this dependency is significantly stronger than that obtained with the true probability and with the estimates obtained with the leaky integrator (see text).

was applied to the true value P_{true} and to the estimate obtained by the leaky integrator.

We quantitatively estimated the Pearson correlation coefficient and the mutual information between the raw data and the different models. First, as we can see in Figure 4-A, the probability bias P_{BBCP} estimated by the BBCP algorithm is linearly correlated with the aSPEM velocity, both as computed on the whole data or for each observer individually (see insets in the Figure). The respective values for the whole dataset ($r = 0.657$ and $MI = 0.687$) and across subjects ($r = 0.673 \pm 0.079$ and $MI = 0.707 \pm 0.134$) are slightly higher than that found by [44] and [12] for aSPEM measures gathered across experimental blocks with fixed direction biases and significantly[1] better than that estimated with the true probability ($r = 0.613 \pm 0.069$ with $p = 0.002$ and $MI = 0.562 \pm 0.107$ with $p = 0.002$) and for that estimated by the leaky-integrator model ($r = 0.600 \pm 0.079$ with $p = 0.003$ and $MI = 0.622 \pm 0.102$ with $p = 0.004$), see inset). A similar analysis illustrates the relationship between the model-estimated probability bias and the rating value, or bet score, about the expected outcome, which was provided at each trial by participants and is shown in Figure 3. Similarly to the aSPEM strength, the rating values are nicely correlated with the probability bias given by the model, as quantified by the Pearson correlation coefficient and mutual information across subjects ($r = 0.813 \pm 0.091$ and $MI = 1.312 \pm 0.364$). Importantly, this value is again higher for the BBCP model than for the leaky integrator ($r = 0.731 \pm 0.129$ with $p = 0.007$ and $MI = 1.117 \pm 0.409$ with $p = 0.028$), or with the true probability ($r = 0.694 \pm 0.086$ with $p = 0.002$ and $MI = 0.940 \pm 0.255$ with $p = 0.002$). Further notice that, in order to account for some specific changes observed in the behavioral data after the short pauses occurring every 50 trials, we added the assumption that there was a switch at each pause. However, removing this assumption did not significantly change the conclusions about the match of the model compared to P_{true} or P_{leaky} both for eye movements (P_{BBCP}: $r = 0.667 \pm 0.078$ and $MI = 0.712 \pm 0.125$, P_{leaky}: $r = 0.548 \pm 0.074$ with $p = 0.003$ and $MI = 0.577 \pm 0.096$ with $p = 0.003$; P_{true} : $r = 0.613 \pm 0.069$ with $p = 0.002$ and $MI = 0.562 \pm 0.107$ with $p = 0.002$) and the bet experiment (P_{BBCP}: $r = 0.802 \pm 0.090$ and $MI = 1.255 \pm 0.349$, P_{leaky}: $r = 0.641 \pm 0.120$ with $p = 0.002$ and $MI = 0.966 \pm 0.300$ with $p = 0.002$; P_{true} : $r = 0.694 \pm 0.086$ with $p = 0.002$ and $MI = 0.940 \pm 0.255$ with $p = 0.002$). To conclude, we deduce that the dynamic estimate of the probability bias produced by the BBCP model is a powerful regressor to explain both the strength of anticipatory smooth pursuit eye movements and the explicit ratings of human observers experiencing a volatile context for visual motion.

This relatively strong correlation is surprising at a first sight as the epochs with constant probability bias (between two switches) have random lengths, and participants have to adapt to such a volatile environment. However, adaptivity to a volatile environment is one of the most exquisite human skills: When faced with some new observations, the observer has to constantly adapt his/her response to either exploit this information by considering that this observation belongs to the same context of the previous observations, or to explore a novel hypothesis about the context. This compromise is one of the crucial component that we wished to explore and which is well captured by the BBCP model. In particular, the model predicts different aspects of the experimental results, from the variability as a function of the inferred probability, to the dynamics of the behavior following a (hidden) switch.

[1] All following p-values are obtained from the Wilcoxon signed-rank test.

4 Results: Analyzing inter-individual differences

So far, we have presented the qualitative behavior of individual participants and we have reported the quantitative analysis of the group-pooled data for the fit between experimental and model-inferred estimates of the hidden probability bias. For instance, the experimental measures for two representative participants in Figure 3, support the qualitative match between behavioral data and model predictions, which we then confirmed quantitatively on the whole group of participants. It is important to note that no model fitting procedure was used so far, but only the match of the results of the BBCP-model applied to the sequence of binary target directions presented to the human participants, as shown in Figure 2-B. However, we observed that in both sessions the qualitative match between model and data varied across participants. This was best characterized by differences in the variability of the responses, but also, for instance, by the different characteristic delays after a switch. This reflects the spectrum of individual behavioral choices between exploration versus exploration [57]. As a consequence, we were interested in characterizing these individual preferences for each individual participant, but also to investigate whether this preference co-varied across the two experimental sessions (i.e. across implicit vs explicit response modalities). Crucially, we have seen that the BBCP model is controlled by a single parameter, the hazard rate, or equivalently by its inverse, the characteristic time τ. Also, we have shown that knowing an observed sequence of behavioral responses, we could fit the value of h which would best explain the observations, as quantified by the Pearson's correlation coefficient or by the mutual information. Thus, by extracting the best-fit parameters for each participant and experimental session we expect to better understand the variety of inter individual differences.

Hence, we have fitted the sequence of responses generated by each participant and for each experimental session, that is for the eye movements and the rating scale experiments. To avoid any possible bias from the fitting procedure, we tested 1600 linearly spaced values of τ from 1 to 1600 trials. For each, we computed the correlation coefficient with the BBCP-model responses parameterized by the value of the hazard rate $h = \frac{1}{\tau}$. We then extracted different estimates of h_{aSPEM} and h_{bet}, respectively for aSPEM and the rating scale, by choosing the hazard rate value corresponding to that with maximal correlation coefficient. To cross-validate our results for each individual participant, we have fitted the BBCP model to each of the 3 sub-blocks of 200 trials. This provides with 3 values of the best fitted hazard rate for each session and observer. The scatter plot of the best fit values is shown in Figure 5. This figure suggests, in the first place, that there is some variability in the best fitted value of the hazard rate in both sessions. Overall, the value of correlation coefficient of the best fit hazard rate was slightly higher than that computed in Figure 3 with $r = 0.682 \pm 0.080$ for the eye movement session and $r = 0.811 \pm 0.089$ for the rating scale session. A part of the variability in the estimated hazard rates comes from the limited length of the data blocks, while another part is due to intra-individual and inter-individual variabilities. Overall, the median (with 25% and 75% quantiles) are $h_{\text{aSPEM}} = 0.069$ $(0.038, 0.093)$ for the aSPEM session and $h_{\text{bet}} = 0.025$ $(0.011, 0.093)$ for the rating scale. We observe that these values are close to the (hidden) ground truth value ($h = 1/40 = 0.025$) used to generate the sequence. In addition, the best-fit hazard rate value is higher for aSPEM compared to the true value and the rating scale measures. In addition, we observed a tendency for hazard rate to be higher in the eye movement recording session. As a consequence, this analysis reveals that relaxing the free parameter of the BBCP model improves the match of the model to the behavioral data and that we could represent the distribution of individual differences in the choice behavior between exploration and exploitation in both sessions for each subject.

The distribution of best-fitted values for each individual subject seemed to

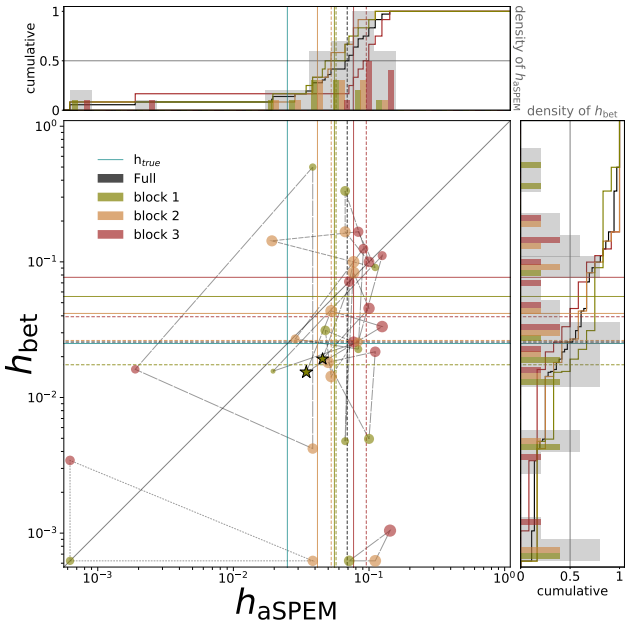

Fig 5. Analysis of inter-individual differences. We analyzed each participant's behavior individually, by searching the individual best value of the model's single free parameter, the hazard rate h. Estimates were performed independently on both experiments, such that we extracted different estimates of h_{aSPEM} and h_{bet} respectively for the aSPEM strength and the rating value. The dots correspond to independent estimates of the hazard rate in each 200 trial sub-block and data belonging to each individual participant are joined by dotted lines. Dashed lines correspond to the median for the full dataset (black line) or for each individual sub-block (colored line). These should be compared to the values obtained for the BBCP model, showing a slight variability over sub-blocks. Stars correspond to the observers displayed in Figure 3. This plot shows that best fit hazard rates are in general higher than the ground truth (blue line), and in general higher for eye movements (below the diagonal). Note that the histograms of hazard-rate best-fit estimates (grey shaded areas) is much more narrower for the eye movement session than for the bet experiment, as also illustrated by the cumulative distributions (plain lines in black or colors). Such an analysis suggests that participants ultimately have different mechanisms at the unconscious and conscious levels for guiding their tendency of exploration versus exploitation.

qualitatively cluster, but the dataset is still insufficiently large to support the significance of such observation at a quantitative level. Moreover, there is a difference in the distribution of observed hazard rates in both sessions. Indeed, we observed that the marginal distribution for each session is different, with the distribution in the aSPEM session being narrower than that observed for the rating scale session. In particular, we also observed the same behavior for each sub-block independently, suggesting that the origin of this variability mainly comes from inter-subject variability. Such an analysis suggests that even though the predictive processes at work in both sessions may reflect a common origin for the evaluation of volatility, this estimation is then more strongly modulated by individual preferences when a more conscious cognitive process is at stake.

5 Discussion

The capacity to adapt our behavior to the environmental regularities has been investigated in different research fields, from motor priming and sensory adaptation to reinforcement learning, machine learning and economics. Several studies have aimed at characterizing the typical time scale over which such adaptation occurs. However, the pattern of environmental regularities could very well change in time, thereby making a fixed time-scale for adaptation a suboptimal cognitive strategy. In addition, different behaviors are submitted to different constraints and respond to different challenges, thus it is reasonable to expect some differences in the way (and time scales) they adapt to the changing environment. This study is an attempt to address these crucial open questions. We have taken an original approach, by assuming a theoretically-defined volatility in the properties of the environment (in the specific context of visual motion tracking) and we have developed an optimal inferential agent, which best captures the hidden properties of the generative model solely based on the trial sequence of target motion. We have then compared the optimal agent's prediction, as well as a more classical *forgetful agent*, to two sets of behavioral data, one rooted in the early visuomotor loop underlying anticipatory ocular tracking, and the other related to the explicit, conscious estimate of the likelihood of a future event. Our results point to a flexible adaptation strategy in humans, taking into account the volatility of the environmental statistics. The time-scale of this dynamic adaptive process would thus vary across time, but it would also be modulated by the specific behavioral task and by inter-individual differences. In this section we discuss the present work and its implications in view of the existing literature and some general open questions.

5.1 Environmental regularities, cognitive properties and visual perception

The time-varying statistical regularities that characterize the environment are likely to influence several cognitive functions. In this study, we have made the choice to focus on a largely unconscious motor behavior (aSPEM), as well as on the explicit rating of expectation for the forthcoming motion direction. In contrast, we have not addressed the question of whether and how statistical learning affects visual motion perception throughout our model-generated volatile sequences. In an empirical context similar to ours, [11] have recently shown that perceptual adaptation for speed estimation occurs concurrently to priming-based aSPEM throughout a sequence of motion tracking trials with randomly varying speed. They actually found a robust *repulsive* adaptation effect, with perceptual judgements biased in favor of faster percepts after seeing stimuli that were slower and *vice-versa*. Concurrently, these authors also found a positive effect on anticipatory smooth pursuit, with faster anticipation after faster stimuli, somehow in agreement with the adaptive properties of aSPEM that we also report here. [11]

quantified the trial-history effects on aSPEM and speed perception by fitting a fixed-size memory model similar to the forgetful agent. They found that aSPEM and speed perception change over different time scales, with the priming effects being maximized for short-term stimulus history (around 2 trials) and adaptation for longer stimulus history, around 15 trials. Their main conclusion was that perceptual adaptation and oculomotor priming are the result of two distinct readout processes using the same internal representation of motion regularities. Note that both these history lengths can be considered short in comparison to the several hundreds of trials that are commonly used in psychophysics and sensorimotor adaptation studies and that, similar to the present study, the inferred characteristic times are even shorter for the buildup of anticipatory eye movements. However, it is also important to note that in the study by [11], the generative model underlying the random sequence of motion trials was different and much simpler than in the present study: In particular the role of environmental volatility was not directly addressed there. This makes a direct comparison between their results and ours difficult beyond a qualitative level.

In spite of a multitude of existing studies investigating the dynamics of sequential effects on visual perception (see for example [6, 8]), only few of them have directly addressed the role of the environmental volatility on the different behavioral outcomes. [28] have compared the predictions of different models, featuring a dynamic adaptation to the environment's volatility (equivalent to our *forgetful agent model*) versus a fixed belief model, on five sets of previously acquired data, including reaction time, explicit reports and neurophysiological measures. Interestingly, [28] concluded that the estimation of a time-varying transition probability matrix constitutes a core building block of sequence knowledge in the brain, which then applies to a variety of sensory modalities and experimental situations. As such, sequential effects in binary sequences would be better explained by learning and updating transition probabilities compared to the absolute item frequencies (as in the present work) or the frequencies of their alternations. The critical difference lies in the content of what is learned (transition probabilities versus item frequencies) in an attempt to capture human behavior. Rather than on transition probabilities, here we focused on the analysis and modeling of human behavior as a function of the frequency of presentation (and its fluctuations in time) of a given event in a binary sequence of alternating visual motion direction. We can speculate that different statistics can play a different role depending on the context, but altogether the study by [28] and the present one converge to highlight the importance of a dynamic estimate of the hierarchical statistical properties of the environment for efficient behavior. There are also other limits to the agent that we have defined. In this study we assume that data are provided as a sequence of discrete steps. A similar approach using a Poisson point process allows to extend our model to the continuous time domain, such as addressed by [65]: In their experiments, the authors analyzed the licking behavior of rats in a dynamic environment. The generalization to the time-continuous case is beyond the scope of our current protocol, but it would consist in a natural extension of it to more complex and ecological settings.

The way expectations act on cognitive processes in general has been investigated in a wide range of domains such as predictive coding [66], active inference [67], motor control [68] and reinforcement learning [12, 57, 62]. Non-stationary observations can also explain why both local and global effects emerge and why local effects persist in the long run even within purely random sequences [20, 32]. This constant update of a general belief on the world can be a consequence of the constant attempt to learn the non-stationary structure of the environment that can change at unpredictable times [20]. Many studies have actually already pointed out the brain's ability to apprehend non-stationary states in environments [64, 69]. Future work will be needed to address the amplitude and dynamics of modulations of visual perception and other cognitive

functions in a model-based volatile environment like the one we formally defined in this study, and to compare them to other implicit and explicit behavioral measures (like anticipatory eye movements and explicit expectation ratings).

5.2 Hierarchical Bayesian inference in the brain

When we perceive the physical world, make a decision or take an action to interact with it, our brain must deal with an ubiquitous property of it, uncertainty. Uncertainty can arise at different levels and be structured around different characteristic time scales. During the past decades, modern science seems to have completed an epistemological transition, from struggling to reduce or neglect uncertainly to engaging in understanding it as a crucial constituent of the world. In the cognitive neurosciences this transition has been formalized in the theoretical framework of Bayesian probabilistic inference, which has become very popular as a benchmark of optimal behavior in perceptual, sensorimotor and cognitive tasks [70] and gives a unified framework for studying the brain [67]. Furthermore, plausible hypotheses about the implementation of Bayesian computations —or approximations of them— in the activity of neuronal populations have been proposed [71–73].

However, one should be careful when evaluating the quality of fit of Bayesian inference models for behavioral data, and avoid any over-interpretation of the results. Note that, if we assume that the inversion of the generative model is perfect (that is, if no algorithmic approximation has been done, like in the present study), this means that by fitting different ideal observers to the data, one evaluates as a matter of fact the adequacy of a specific generative model, not of the probabilistic calculus in its detailed implementation. There is a common confusion around the idea of a "Bayesian brain". We actually believe that the challenge here is not to validate the hypothesis that the brain uses or not the Bayes' theorem, or a more complex hierarchical combinations of inferential computations, but rather to test different hypotheses about the different generative models that agents may use. This methodological point will be essential in designing future experimental protocols, and in evaluating quantitatively the results. The brain is probably only "weakly Bayesian" (it does not care about equations but more about sugar, after all!). One remaining question though, is to understand why in cognitive systems the adaptation to hierarchical probabilistic fluctuations occurs and in particular why it may deviate in some pathological disorders such as schizophrenia [5, 74] or across the natural variability of autistic traits [75].

While it was not our original objective, we have analyzed in this study the individual best-fit parameters (hazard rates) of the BCCP model: despite a consistent variability of such parameters across sub-blocks of the trial sequence, we highlighted some noteworthy tendencies for participants to cluster around specific properties of the dynamic adaptation to a volatile probabilistic environment. Most important, this analysis corroborates and strengthens some recent attempts to realize a *computational phenotyping* of human participants. However, more extensive studied should be conducted to be able to quantitatively titrate inter-individual tendencies.

5.3 Non-linearities in the adaptation to probabilistic environments

Finally, neuroeconomists have pointed out a generic aversion to risk [76] such that the value of a possible outcome is weighted by the precision of the inference, leading in general to an under-weighting of high gains and losses. Importantly, [77] compared a classical economic decision task with a motor decision task: they found that participants were more risk seeking in the motor task compared to the first one. More recently, in a task similar to ours, where the behavioral choice was not specifically

associated to a reward schedule, [47] found a weak non-linearity in the dependence of aSPEM upon the probability of motion direction, yielding an overweight of the extreme values of probability, whereas an opposite non-linearity (underweight) was observed when the target direction was visually-cued with a given probability of validity. In our data we have not found consistent evidence suggesting a clear non-linearity in either sense. Further work is needed to disentangle the possible specificities (e.g. non linearities), in this respect, of different cognitive tasks, as well as to investigate the dependence of non-linearities upon the environmental volatility.

6 Conclusions

- We have developed a Bayesian model of an agent estimating the probability bias of a volatile environment with changing points (switches), such that the agent may decide *to stay* on the current hypothesis about the environment, or *to go* for a novel one. This allows to dynamically infer the probability bias across time and directly compare model predictions and experimental data, such as measures of human behavior.
- We applied such a framework to the case of a probability bias in a visual motion task where we manipulated the target direction probability. We observed a good match between the largely unconscious anticipatory smooth eye movements and the results of the model, replicating and providing a novel solid theoretical framework for previous findings [12, 44, 47].
- We also found a good match between model predictions and the explicit rating of the expected target motion direction, a novel result suggesting that this model captures some of the brain computations underlying expectancy based motion prediction, both at the unconscious and conscious level.
- Finally, we found that the experimental data of each different participant matched to different types of belief about the volatile environment, some being more or less conservative than others. Interestingly, each of the two experiments (namely for the unconscious anticipatory eye movements and the conscious rating) provided different distributions, opening the perspective for future *computational phenotyping* using such a volatile setting.

7 Material and Methods

7.1 Participants, visual stimuli and experimental design

Twelve observers (29 years old ± 5.15, 7 female) with normal or corrected-to-normal vision took part in these experiments. They gave their informed consent and the experiments had received ethical approval from the Aix-Marseille Ethics Committee (approval 2014-12-3-05), in accordance with the declaration of Helsinki.

Visual stimuli were generated using PsychoPy 1.85.2 [78] on a Mac running OS 10.6.8 and displayed on a 22" Samsung SyncMaster 2233 monitor with 1680×1050 pixels resolution at 100 Hz refresh rate. Experimental routines also written using PsychoPy controlled the stimulus display. Observers sat 57 cm from the screen in a dark room.

The moving target used in our experiments was a white ring (0.35° outer diameter and 0.27° inner diameter) with a luminance of 102 $cd/m2$ that moved horizontally on a grey background (luminance 42 cd/m^2). Each trial started with a central fixation point displayed for a random duration drawn from a uniform distribution ranging between 400 and 800 ms. Then a fixed-duration 300 ms gap occurred between the offset of the fixation point and the onset of the moving target, which was presented slightly offset

from the fixation location [79] and immediately started moving horizontally at a constant speed of $15°/s$, either to the right or to the left for 1000 ms. The probability p of rightward trials was a time-varying random variable which was constant within an epoch of the sequence of a given random size (see main text for the description of the generative model).

The paradigm included two experimental sessions performed on two distinct (in general consecutive) days by each participant. The two sessions involved the presentation of the same sequence of trials, while collecting a different behavioral response: explicit rating judgments in the first session (the *bet* experiment), and eye movement recordings in the second session. Asked after the experiment, no observer noticed that the same (pseudo-)random sequence of target directions was used in both experiments.

7.2 Eye movements experiment

Eye movements were recorded continuously with an eye tracking system (Eyelink 1000, SR Research Ltd., sampled at 1000 Hz), using the Python module Pylink 0.1.0 provided by PsychoPy. Horizontal and vertical eye position data were transferred, stored, and analyzed offline using programs written using Jupyter notebooks. To minimize measurement errors, the participant's head movements were restrained using a chin and forehead rest, so that the eyes in primary gaze position were directed towards the center of the screen. In order to enforce accuracy in gaze position and tracking, we implemented an automatic procedure of fixation control. If the distance between the gaze position and the central fixation point during the fixation epoch exceeded 2° of visual angles, the fixation point started flickering and the counter for the fixation duration was reset to 0.

The recorded horizontal and vertical raw gaze position data were numerically differentiated to obtain velocity measures. We adopted an automatic conjoint acceleration and velocity threshold method (the default saccade detection implemented by SR Research) to detect ocular saccades. Saccades and eye-blinks were excluded from eye velocity traces (and replaced by *Not-a-Number* values in the numerical arrays) before trial averaging and data fitting for the extraction of the oculomotor parameters of interest. In order to extract the relevant parameters of the oculomotor responses, we developed new tools based on a best-fitting procedure of predefined oculomotor patterns and in particular the typical smooth pursuit velocity profile that was recorded in our experiment. A piecewise-defined function was fitted to the different epochs of the eye velocity traces: a constant function during fixation, a ramp-like linear function during smooth pursuit anticipation, an increasing sigmoid-function during the initiation of visually-guided smooth pursuit, reaching its saturating value during the pursuit steady-state. This analysis was applied to each trial individually and it allowed in particular to estimate the anticipatory smooth pursuit velocity. Some trials were excluded from the analysis as the proportion of missing data-points, due to eye blinks or saccades was considered too large, namely when the missing data exceeded 45 ms during the gap or one third of the total target motion epoch (4.36% of all trials). In addition, trials were also excluded when the eye-movement fitting procedure did not converge, after visual inspection, to a satisfactory match with the data (3.25% of all trials). The python scripts used to analyze eye movements are available at `https://github.com/invibe/ANEMO`.

7.3 The Bet experiment

The aim of the Bet experiment was to collect data related to the individual conscious estimates of the probability of target motion direction. At the beginning of each trial,

before the presentation of the moving target, participants had to answer to the question *"How sure are you that the target will go left or right"*. This was performed by adjusting a cursor on the screen using the mouse (see Figure Figure 1-C). The cursor could be placed at any point along a horizontal segment representing a linear rating scale with three ticks labeled as *"Left"*, *"Right"* (at the extreme left and right end of the segment respectively), and *"Unsure"* in the middle. Participants had to validate their choice by clicking on the mouse left-button and the actual target motion was shown thereafter. The rationale to collect rating responses on a continuous scale instead of a simple binary prediction (Right/Left) was to be able to infer the individual estimate of the direction bias at the single trial scale (in analogy to the continuous interval for the strength of aSPEM velocity). We called this experiment the *"Bet"* experiment, as participants were explicitly encouraged to make reasonable rating estimates, as though they had to bet money on the next trial outcome. Every 50 trials, a *"score"* was displayed on the screen, corresponding to the proportion of correct direction predictions (Right or Left of the *"Unsure"* tick) weighted by the confidence attributed to each answer (the distance of the cursor from the center).

Acknowledgments

This work was supported by EU Marie-Sklodowska-Curie Grant No 642961 (PACE-ITN) and by the Fondation pour le Recherche Médicale, under the program *Equipe FRM* (DEQ20180339203/PredictEye/G Masson). Code and material on the corresponding author's website. We thank Doctor Jean-Bernard Damasse, Guillaume S Masson and Professor Laurent Madelain for insightful discussions.

References

1. Perrinet LU, Adams RA, Friston KJ. Active inference, eye movements and oculomotor delays. Biological Cybernetics. 2014;108(6):777–801. doi:10.1007/s00422-014-0620-8.

2. Barack DL, Gold JI. Temporal Trade-Offs in Psychophysics. Current opinion in neurobiology. 2016;37:121–125. doi:10.1016/j.conb.2016.01.015.

3. Cohen JD, McClure SM, Yu AJ. Should I stay or should I go? How the human brain manages the trade-off between exploitation and exploration. Philosophical Transactions of the Royal Society of London B: Biological Sciences. 2007;362(1481):933–942.

4. Sotiropoulos G, Seitz AR, Seriès P. Changing Expectations about Speed Alters Perceived Motion Direction. Current Biology. 2011;21(21):R883—-R884. doi:10.1016/j.cub.2011.09.013.

5. Adams RARA, Perrinet LU, Friston KKKJ, Dayan P, Friston KKKJ. Smooth pursuit and visual occlusion: active inference and oculomotor control in schizophrenia. PloS one. 2012;7(10):e47502. doi:10.1371/journal.pone.0047502.

6. Chopin A, Mamassian P. Predictive Properties of Visual Adaptation. Current Biology. 2012;22(7):622–626. doi:10.1016/j.cub.2012.02.021.

7. Fischer J, Whitney D. Serial dependence in visual perception. Nature Neuroscience. 2014;17(5):738–743. doi:10.1038/nn.3689.

8. Cicchini GM, Mikellidou K, Burr DC. The functional role of serial dependence. Proceedings of the Royal Society B: Biological Sciences. 2018;285(1890):20181722. doi:10.1098/rspb.2018.1722.

9. Wallman J, Fuchs AF. Saccadic Gain Modification: Visual Error Drives Motor Adaptation. Journal of Neurophysiology. 1998;80(5):2405–2416. doi:10.1152/jn.1998.80.5.2405.

10. Carpenter RH, Williams ML. Neural Computation of Log Likelihood in Control of Saccadic Eye Movements. Nature. 1995;377(6544):59–62. doi:10/bjktb8.

11. Maus GW, Potapchuk E, Watamaniuk SNJ, Heinen SJ. Different Time Scales of Motion Integration for Anticipatory Smooth Pursuit and Perceptual Adaptation. Journal of Vision. 2015;15(2). doi:10.1167/15.2.16.

12. Damasse JB, Perrinet LU, Madelain L, Montagnini A. Reinforcement effects in anticipatory smooth eye movements. Journal of Vision. 2018;doi:10.1167/18.11.14.

13. Clifford CWG, Webster MA, Stanley GB, Stocker AA, Kohn A, Sharpee TO, et al. Visual adaptation: Neural, psychological and computational aspects. Vision Research. 2007;47(25):3125–3131. doi:10.1016/j.visres.2007.08.023.

14. Webster MA. Adaptation and visual coding. Journal of Vision. 2011;11(5):3–3. doi:10.1167/11.5.3.

15. Kohn A, Kohn A. Visual Adaptation: Physiology, Mechanisms, and Functional Bene ts. Journal of Neurophysiology. 2007;10461:3155–3164. doi:10.1152/jn.00086.2007.

16. Kanai R, Verstraten FAJ. Perceptual manifestations of fast neural plasticity: Motion priming, rapid motion aftereffect and perceptual sensitization. Vision Research. 2005;45(25-26):3109–3116. doi:10.1016/J.VISRES.2005.05.014.

17. Verstraten FAJ, Fredericksen RE, Grüsser OJ, Van De Grind WA. Recovery from motion adaptation is delayed by successively presented orthogonal motion. Vision Research. 1994;34(9):1149–1155. doi:10.1016/0042-6989(94)90297-6.

18. Tiest WMB, Kappers AML. Tactile perception of thermal diffusivity. Attention, perception & psychophysics. 2009;71(3):481–489. doi:10.3758/APP.

19. Hyman R. Stimulus information as a determinant of reaction time. Journal of Experimental Psychology. 1953;45(3):188–196. doi:10.1037/h0056940.

20. Yu AJ, Cohen JD. Sequential effects: Superstition or rational behavior? Advances in Neural Information Processing Systems. 2009;21:1873–80.

21. Deneve S, Latham PE, Pouget A. Reading population codes: a neural implementation of ideal observers. Nature neuroscience. 1999;2(8):740–5. doi:10.1038/11205.

22. Diaconescu AO, Mathys C, Weber LAE, Daunizeau J, Kasper L, Lomakina EI, et al. Inferring on the Intentions of Others by Hierarchical Bayesian Learning. PLoS Computational Biology. 2014;10(9). doi:10.1371/journal.pcbi.1003810.

23. Daunizeau J, den Ouden HEM, Pessiglione M, Kiebel SJ, Stephan KE, Friston KJ. Observing the Observer (I): Meta-Bayesian Models of Learning and Decision-Making. PLoS ONE. 2010;5(12):e15554. doi:10.1371/journal.pone.0015554.

24. Hoyer PO, Hyvarinen A. Interpreting neural response variability as Monte Carlo sampling of the posterior. Advances in neural information processing systems. 2003;(1):293–300. doi:10.1.1.71.1731.

25. Ma WJ, Jazayeri M. Neural Coding of Uncertainty and Probability. Annual Review of Neuroscience. 2014;37(1):205–220. doi:10.1146/annurev-neuro-071013-014017.

26. Jaynes ET. Probability Theory: The Logic of Science. 1. Cambridge university press; 2014.

27. Montagnini A, Mamassian P, Perrinet L, Castet E, Masson GS. Bayesian modeling of dynamic motion integration. Journal of physiology, Paris. 2007;101(1-3):64–77. doi:10.1016/j.jphysparis.2007.10.013.

28. Meyniel F, Maheu M, Dehaene S. Human Inferences about Sequences: A Minimal Transition Probability Model. PLoS Computational Biology. 2016;12(12):1–26. doi:10.1371/journal.pcbi.1005260.

29. Squires KC, Wickens C, Squires K, Donchin E. The Effect of Stimulus Sequence. Science. 1976;193(6):1142–1146.

30. Huettel SA, Mack PB, McCarthy G. Perceiving patterns in random series: Dynamic processing of sequence in prefrontal cortex. Nature Neuroscience. 2002;5(5):485–490. doi:10.1038/nn841.

31. Kolossa A, Fingscheidt T, Wessel K, Kopp B. A Model-Based Approach to Trial-By-Trial P300 Amplitude Fluctuations. Frontiers in Human Neuroscience. 2013;6(February):1–18. doi:10.3389/fnhum.2012.00359.

32. Cho R, Nystrom L, Jones a, Braver T, Holmes P, Cohen J. Mechanisms underlying performance dependencies on stimulus history in a two-alternative forced choice task. Cog Aff Behav Neurosci. 2002;2(412):283–299.

33. Falk R, Konold C. Making Sense of Randomness: Implicit Encoding as a Basis for Judgment. Psychological Review. 1997;104(2):301–318. doi:10.1037/0033-295X.104.2.301.

34. Krauzlis RJ. Eye Movements. In: Squires, L R and Berg D, editor. Fundamental Neuroscience. 3rd ed. Amsterdam, NL: Elsevier; 2008.

35. Krauzlis RJ, Lisberger SGS. A control systems model of smooth pursuit eye movements with realistic emergent properties. Neural Computation. 1989;1(1):116–122. doi:10.1162/neco.1989.1.1.116.

36. Westheimer G. Eye movement responses to a horizontally moving visual stimulus. AMA Archives of Ophthalmology. 1954;52(6):932–941. doi:10.1001/archopht.1954.00920050938013.

37. Kowler E, Steinman R. The effect of expectations on slow oculomotor control-I. Periodic target steps. Vision Research. 1979;19(6):619 – 632. doi:https://doi.org/10.1016/0042-6989(79)90238-4.

38. Kowler E, Steinman RM. The effect of expectations on slow oculomotor control—II. Single target displacements. Vision Research. 1979;19(6):633 – 646. doi:https://doi.org/10.1016/0042-6989(79)90239-6.

39. Badler JB, Heinen SJ. Anticipatory Movement Timing Using Prediction and External Cues. Journal of Neuroscience. 2006;26(17):4519–4525. doi:10.1523/JNEUROSCI.3739-05.2006.

40. Becker W, Fuchs aF. Prediction in the oculomotor system: smooth pursuit during transient disappearance of a visual target. Experimental Brain Research. 1985;57:562–575. doi:10.1007/BF00237843.

41. Orban de Xivry JJ, Missal M, Lefevre P. A dynamic representation of target motion drives predictive smooth pursuit during target blanking. Journal of Vision. 2008;8(15):6–6. doi:10.1167/8.15.6.

42. Kowler E, Martins AJ, Pavel M. The effect of expectations on slow oculomotor control-IV. Anticipatory smooth eye movements depend on prior target motions. Vision Research. 1984;24(3):197–210. doi:10.1016/0042-6989(84)90122-6.

43. Deravet N, Blohm G, de Xivry JJO, Lefèvre P. Weighted integration of short-term memory and sensory signals in the oculomotor system. Journal of Vision. 2018;18(5):16. doi:10.1167/18.5.16.

44. Montagnini A, Souto D, Masson GS. Anticipatory eye-movements under uncertainty: a window onto the internal representation of a visuomotor prior. Journal of Vision. 2010;10(7):554a.

45. Kowler E. Cognitive expectations, not habits, control anticipatory smooth oculomotor pursuit. Vision Research. 1989;29(9):1049–1057. doi:10.1016/0042-6989(89)90052-7.

46. Heinen SJ, Badler JB, Ting W. Timing and velocity randomization similarly affect anticipatory pursuit. Journal of Vision. 2005;5(6):1–1. doi:10.1167/5.6.1.

47. Santos EM, Kowler E. Anticipatory smooth pursuit eye movements evoked by probabilistic cues. Journal of Vision. 2017;17(2017):1–16. doi:10.1167/17.13.13.doi.

48. Kowler E, Aitkin C, Ross N. Davida Teller Award Lecture 2013: The importance of prediction and anticipation in the control of smooth pursuit eye movements. Journal of . . . . 2014;14:1–16. doi:10.1167/14.5.10.doi.

49. Fukushima K, Tanaka M, Suzuki Y, Fukushima J, Yoshida T. Adaptive Changes in Human Smooth Pursuit Eye Movement. Neuroscience research. 1996;25(4):391–398. doi:10/ff6s3h.

50. Kahlon M, Lisberger SG. Coordinate System for Learning in the Smooth Pursuit Eye Movements of Monkeys. The Journal of neuroscience : the official journal of the Society for Neuroscience. 1996;16(22):7270–7283.

51. Souto D, Kerzel D. Like a rolling stone: Naturalistic visual kinematics facilitate tracking eye movements. Journal of Vision. 2013;13(2):9–9. doi:10.1167/13.2.9.

52. Mathys C, Daunizeau J, Friston KJ, Stephan KE. A bayesian foundation for individual learning under uncertainty. Frontiers in human neuroscience. 2011;5(May):39. doi:10.3389/fnhum.2011.00039.

53. Vossel S, Mathys C, Daunizeau J, Bauer M, Driver J, Friston KJ, et al. Spatial Attention, Precision, and Bayesian Inference: A Study of Saccadic Response Speed. Cerebral Cortex. 2014;24(6):1436–1450. doi:10.1093/cercor/bhs418.

54. Meyniel F, Sergent C, Rigoux L, Daunizeau J, Pessiglione M. Neurocomputational account of how the human brain decides when to have a break. Proceedings of the National Academy of Sciences of the United States of America. 2013;110(7):2641–2646. doi:10.1073/pnas.1211925110.

55. Adams RP, MacKay DJC. Bayesian Online Changepoint Detection. ArXiv e-prints. 2007;.

56. Anderson AJ, Carpenter RHS. Changes in expectation consequent on experience , modeled by a simple , forgetful neural circuit. Journal of Vision 2006. 2006;6:822–835. doi:10.1167/6.8.5.

57. Behrens TEJ, Woolrich MW, Walton ME, Rushworth MFS. Learning the value of information in an uncertain world. Nature Neuroscience. 2007;10(9):1214–1221. doi:10.1038/nn1954.

58. Vilares I, Kording K. Bayesian models: The structure of the world, uncertainty, behavior, and the brain. Annals of the New York Academy of Sciences. 2011;1224(1):22–39. doi:10.1111/j.1749-6632.2011.05965.x.

59. Schütz AC, Kerzel D, Souto D. Saccadic Adaptation Induced by a Perceptual Task. Journal of Vision. 2014;14(5):4–4. doi:10/f56tvm.

60. Norton EH, Acerbi L, Ma WJ, Landy MS. Human Online Adaptation to Changes in Prior Probability. PLOS Computational Biology doi: 101371/journalpcbi1006681. 2018; p. 483842. doi:10/gfrhgk.

61. Nassar MR, Wilson RC, Heasly B, Gold JI. An Approximately Bayesian Delta-Rule Model Explains the Dynamics of Belief Updating in a Changing Environment. Journal of Neuroscience. 2010;30(37):12366–12378. doi:10.1523/JNEUROSCI.0822-10.2010.

62. Wilson RC, Nassar MR, Gold JI, Behrens T. A Mixture of Delta-Rules Approximation to Bayesian Inference in Change-Point Problems. PLoS Comput Biol. 2013;9(7). doi:10.1371/journal.pcbi.1003150.

63. Glaze CM, Kable JW, Gold JI. Normative Evidence Accumulation in Unpredictable Environments. eLife. 2015;4:e08825. doi:10/gf7rb6.

64. Meyniel F, Schlunegger D, Dehaene S. The Sense of Confidence during Probabilistic Learning: A Normative Account. PLOS Computational Biology. 2015;11(6):1–25. doi:10.1371/journal.pcbi.1004305.

65. Radillo AE, Veliz-Cuba A, Josić K, Kilpatrick ZP. Evidence accumulation and change rate inference in dynamic environments. Neural computation. 2017;29(6):1561–1610.

66. Wacongne C, Changeux JP, Dehaene S. A Neuronal Model of Predictive Coding Accounting for the Mismatch Negativity. Journal of Neuroscience. 2012;32(11):3665–3678. doi:10.1523/JNEUROSCI.5003-11.2012.

67. Friston K. The free-energy principle: A unified brain theory? Nature Reviews Neuroscience. 2010;11(2):127–138. doi:10.1038/nrn2787.

68. Wolpert DM, Ghahramani Z. Computational principles of movement neuroscience. Nature Neuroscience. 2000;3(S11):1212–1217. doi:10.1038/81497.

69. Ossmy O, Moran R, Pfeffer T, Tsetsos K, Usher M, Donner TH. The Timescale of Perceptual Evidence Integration Can Be Adapted to the Environment. Current Biology. 2013;23(11):981–986. doi:10.1016/j.cub.2013.04.039.

70. Knill DC, Pouget A. The Bayesian brain: the role of uncertainty in neural coding and computation. Trends in Neurosciences. 2004;27(12):712–719. doi:10.1016/j.tins.2004.10.007.

71. Bastos AM, Usrey WM, Adams RA, Mangun GR, Fries P, Friston KJ. Canonical microcircuits for predictive coding. Neuron. 2012;76(4):695–711. doi:10.1016/j.neuron.2012.10.038.

72. Fetsch CR, Pouget A, DeAngelis GC, Angelaki DE. Neural correlates of reliability-based cue weighting during multisensory integration. Nature Neuroscience. 2012;15(1):146–154. doi:10.1038/nn.2983.

73. Ma WJ, Beck JM, Latham PE, Pouget A. Bayesian inference with probabilistic population codes. Nature Neuroscience. 2006;9(11):1432–1438. doi:10.1038/nn1790.

74. Jardri R, Duverne S, Litvinova AS, Denève S. Experimental evidence for circular inference in schizophrenia. Nature Communications. 2017;8(1):14218. doi:10.1038/ncomms14218.

75. Karvelis P, Seitz AR, Lawrie SM, Seriès P. Autistic traits, but not schizotypy, predict increased weighting of sensory information in Bayesian visual integration. eLife. 2018;7. doi:10.7554/eLife.34115.

76. Kahneman D, Tversky A. Prospect theory: An analysis of decision under risk. In: Handbook of the fundamentals of financial decision making: Part I. World Scientific; 2013. p. 99–127.

77. Wu SW, Delgado MR, Maloney LT. Economic decision-making compared with an equivalent motor task. Proceedings of the National Academy of Sciences. 2009;106(15):6088–6093. doi:10.1073/PNAS.0900102106.

78. Peirce J, Gray JR, Simpson S, MacAskill M, Höchenberger R, Sogo H, et al. PsychoPy2: Experiments in Behavior Made Easy. Behavior Research Methods. 2019;51(1):195–203. doi:10/gft89w.

79. Rashbass C. The relationship between saccadic and smooth tracking eye movements. The Journal of Physiology. 1961;159(2):326–338. doi:10.1113/jphysiol.1961.sp006811.

8 Supporting information

8.1 Appendix : leaky integrator

Given a series of observations $\{x_0^i\}_{0\leq i\leq t}$ with $\forall i, x_0^i \in \{0,1\}$, we defined

$$\begin{aligned}\hat{x_1}^t &= (1-1/\tau)^{t+1}\cdot \hat{x_1}^{t=0} + 1/\tau \cdot \sum_{0\leq i\leq t}(1-1/\tau)^i \cdot x_0^{t-i} \\ &= (1-h)^{t+1}\cdot \hat{x_1}^{t=0} + h \cdot \sum_{0\leq i\leq t}(1-h)^i \cdot x_0^{t-i}\end{aligned}$$

If we write it for trial $t-1$, we have

$$\begin{aligned}
\hat{x_1}^{t-1} &= (1-h)^t \cdot \hat{x_1}^{t=0} + h \cdot \sum_{0 \leq i \leq t-1} (1-h)^i \cdot x_0^{t-1-i} \\
&= (1-h)^t \cdot \hat{x_1}^{t=0} + h \cdot \sum_{1 \leq j \leq t} (1-h)^{j-1} \cdot x_0^{t-j} \\
(1-h) \cdot \hat{x_1}^{t-1} &= (1-h)^{t+1} \cdot \hat{x_1}^{t=0} + h \cdot \sum_{1 \leq i \leq t} (1-h)^i \cdot x_0^{t-i}
\end{aligned}$$

As such, the integrative formula above becomes an iterative relation:

$$\begin{aligned}
\hat{x_1}^{t} &= (1-h)^{t+1} \cdot \hat{x_1}^{t=0} + h \cdot \sum_{0 \leq i \leq t} (1-1/\tau)^i \cdot x_0^{t-i} \\
&= (1-h)^{t+1} \cdot \hat{x_1}^{t=0} + h \cdot x_0^t + h \cdot \sum_{1 \leq i \leq t} (1-h)^i \cdot x_0^{t-i} \\
&= h \cdot x_0^t + (1-h) \cdot \hat{x_1}^{t-1}
\end{aligned}$$

such that finally

$$\hat{x_1}^{t} = (1-h) \cdot \hat{x_1}^{t-1} + h \cdot x_0^t$$

As such, the definitions in Equation 2 and Equation 3 are equivalent.

8.2 The Bernoulli, binomial and Beta distributions

Let us define some basic concepts. A Bernoulli trial is the outcome of a binary random variable x knowing a probability bias μ (with $0 \geq \mu \geq 1$) and can be formalized as:

$$Pr(x|\mu) = \mu^x \cdot (1-\mu)^{1-x}$$

The binomial distribution is defined as the probability that the sum X of ν independent Bernoulli trials is k:

$$\Pr(k; \nu, \mu) = \Pr(X = k) = \binom{\nu}{k} \cdot \mu^k \cdot (1-\mu)^{\nu-k}$$

Knowing such a model for X it can be of interest to find an estimate of the parameter of the Bernoulli trial, that is of the probability bias μ. This distribution function is called the conjugate of the binomial distribution which is the Beta-distribution. For example, the beta distribution can be used in Bayesian analysis to describe initial knowledge concerning probability of success such as the probability that a product will successfully complete a stress test. The beta distribution is a suitable model for the random behavior of percentages and proportions.

It is usually defined using shape parameters α and β:

$$Pr(p|\alpha, \beta) = \frac{1}{B(\alpha, \beta)} \cdot p^{\alpha-1} \cdot (1-p)^{\beta-1}$$

Note that here, the variable is the probability bias p. The normalization constant $B(\alpha, \beta)$ is given by the beta function. By definition:

$$\alpha = \mu \cdot \nu$$
$$\beta = (1-\mu) \cdot \nu$$

Inversely, $\alpha + \beta = \nu$ and $\mu = \frac{\alpha}{\alpha+\beta} = 1 - \frac{\beta}{\alpha+\beta}$

8.3 Appendix 2: BBCP algorithm

To summarize, the algorithm that we presented is an implementation of the "Bayesian Online Changepoint Detection" by [55] extended for the class of binary inputs. Using the definition of the run-length Section 2.2, the flow-chart of the algorithm is:

1. Initialize
   - $P(r_0 > 0) = 0$ or $P(r_0 = 0) = 1$ and
   - $\mu_0^{(0)} = \mu_{prior}$ and $\nu_0^{(0)} = \nu_{prior}$
2. Observe New Datum $x_0^t \in \{0, 1\}$,
   (a) Evaluate Predictive Probability $\pi_t^{(r)} = P(x_0^t | \mu_t^{(r)}, \nu_t^{(r)})$.
   (b) Calculate Growth Probabilities
   $P(r_t = r_{t-1} + 1, x_{0:t}) = P(r_{t-1}, x_{0:t-1}) \pi_t^{(r)} (1-h)$,
   (c) Calculate Changepoint Probabilities
   $P(r_t = 0, x_{0:t}) = \sum_{r_{t-1}} P(r_{t-1}, x_{0:t-1}) \pi_t^{(r)} \cdot h$,
   (d) Calculate Evidence $P(x_{0:t}) = \sum_{r_{t-1}} P(r_t, x_{0:t})$,
   (e) Determine Run Length Distribution $P(r_t | x_{0:t}) = P(r_t, x_{0:t}) / P(x_{0:t})$.
3. Update sufficient statistics
   - at a switch $\mu_{t+1}^{(0)} = \mu_{prior}$, $\nu_{t+1}^{(0)} = \nu_{prior}$,
   - else, $\nu_{t+1}^{(r+1)} = \nu_t^{(r)} + 1$ and $\nu_{t+1}^{(r+1)} \cdot \mu_{t+1}^{(r+1)} = \nu_t^{(r)} \cdot \mu_t^{(r)} + x_0^t$.
4. Return to step 2.

In the following, we detail some intermediate steps and highlight some key differences with their implementation. We also provide a python implementation of the algorithm, which is openly available on GitHub.

8.3.1 Initialization

Note that the prior distribution is itself a Beta distribution: $\mathcal{P} \propto B(p; \mu_{prior}, \nu_{prior})$. It will by symmetry be unbiased: $\mu_{prior} = .5$. Concerning the shape, it can be for instance the uniform distribution $\mathcal{U}$ on $[0, 1]$, that is $\nu_{prior} = 2$ or Jeffrey's prior $\mathcal{J}$, that is $\nu_{prior} = 1$. We chose the latter for the generation of trials as the uniform distribution would yield more sample around .5. Qualitatively, this would result in more difficult task in discriminating a probability bias from another. Jeffrey's prior was more adapted to that task.

8.3.2 Prediction: run-length distribution

The steps to achieve the update rule are:

$$
\begin{aligned}
Pr(x_0^t|x_0^{0:t-1}) &= \sum_{r^t} Pr(x_0^t|r^t, x_0^{0:t-1}) \cdot \beta_t^{(r)} \\
Pr(x_0^t|x_0^{0:t-1}) &= \sum_{r^t} Pr(x_0^t|r^t, x_0^{0:t-1}) \cdot Pr(r^t|x_0^{0:t-1}) \\
\text{with} \quad Pr(r^t|x_0^{0:t-1}) &\propto \sum_{r^{t-1}} Pr(r^t|r^{t-1}) \cdot Pr(x_0^t|r^{t-1}, x_0^{0:t-1}) \cdot Pr(r^{t-1}|x_0^{0:t-2})
\end{aligned}
$$

Finally we obtain Equation 5:

$$
\beta_t^{(r)} \propto \sum_{r^{t-1}} Pr(r^t|r^{t-1}) \cdot Pr(x_0^t|r^{t-1}, x_0^{0:t-1}) \cdot \beta_{t-1}^{(r)}
$$

8.3.3 Prediction: sufficient statistics

The recursive formulation in Equation 9 and Equation 10 comes from the expression

$$
\nu_t^{(r)} \cdot \mu_t^{(r)} = \sum_{i=t-r-1}^{t-1} x_0^i
$$

and therefore

$$
\begin{aligned}
\nu_{t+1}^{(r+1)} \cdot \mu_{t+1}^{(r+1)} &= \sum_{i=t+1-r-1-1}^{t+1-1} x_0^i \\
&= \sum_{i=t-r-1}^{t} x_0^i \\
&= \nu_t^{(r)} \cdot \mu_t^{(r)} + x_0^t
\end{aligned}
$$

8.3.4 Quantitative evaluation

To quantitatively evaluate our results with respect to another probability bias, we computed in Equation 13 the cost as the Kullback-Leibler divergence $\mathrm{KL}(\hat{p}|p)$ between samples $\hat{p}$ and model p under the hypothesis of a Bernoulli trial:

$$
\mathrm{KL}(\hat{p}|p) = \hat{p} \cdot \log\left(\frac{\hat{p}}{p}\right) + (1-\hat{p}) \cdot \log\left(\frac{1-\hat{p}}{1-p}\right). \tag{14}
$$

8.4 Appendix: likelihood function

We want to compute $\mathcal{L}(r|o) = Pr(o|p, r)$ where $o \in \{0, 1\}$ such that we can evaluate Predictive Probability $\pi_{0:t} = P(x_0^t|\mu_t^{(r)}, \nu_t^{(r)})$ in the algorithm above with $\mu_t^{(r)}$ and $\nu_t^{(r)}$ the sufficient statistics at trial t for node (r). The likelihood of observing $o = 1$ is that of a binomial (conjugate of a Beta distribution) of

- mean rate of choosing hypothesis $o = 1$ equal to $\frac{p \cdot r + o}{r+1}$,
- number of choices where $o = 1$ equals to $p \cdot r + 1$.

More generally, by observing o, the new rate is $p^{'} = \frac{p \cdot r + o}{r+1}$.

8.4.1 Mathematical derivation

The likelihood will give the probability of this novel rate given the known parameters and their update (in particular $r^{'} = r + 1$):

$$
\begin{aligned}
L(r|o) &= (\frac{p \cdot r + o}{r+1})^{p \cdot r + o} \cdot (1 - \frac{p \cdot r + o}{r+1})^{r+o-(p \cdot r + o)} \\
&= \frac{1}{(r+1)^{r+1}} \cdot (p \cdot r + o)^{p \cdot r + o} \cdot ((1-p) \cdot r + 1 - o)^{(1-p) \cdot r + 1 - o}
\end{aligned}
$$

since both likelihood sum to 1, the likelihood of drawing o in the set $\{0, 1\}$ is equal to

$$
\begin{aligned}
\mathcal{L}(r|o) &= \frac{L(r|o)}{L(r|o=1) + L(r|o=0)} \\
&= \frac{(p \cdot r + o)^{p \cdot r + o} \cdot ((1-p) \cdot r + 1 - o)^{(1-p) \cdot r + 1 - o}}{(p \cdot r + 1)^{p \cdot r + 1} \cdot ((1-p) \cdot r)^{(1-p) \cdot r} + (p \cdot r)^{p \cdot r} \cdot ((1-p) \cdot r + 1)^{(1-p) \cdot r + 1}} \\
&= \frac{(1-o) \cdot (p \cdot r)^{p \cdot r} \cdot ((1-p) \cdot r + 1)^{(1-p) \cdot r + 1} + o \cdot (p \cdot r + 1)^{p \cdot r + 1} \cdot ((1-p) \cdot r)^{(1-p) \cdot r}}{(p \cdot r + 1)^{p \cdot r + 1} \cdot ((1-p) \cdot r)^{(1-p) \cdot r} + (p \cdot r)^{p \cdot r} \cdot ((1-p) \cdot r + 1)^{(1-p) \cdot r + 1}}
\end{aligned}
$$

This can also be written by isolating the part which depends on o and for a given run-length and knowing sufficient statistics describing the sufficient statistics at each node r:

$$
\mathcal{L}(r|o) = \frac{1}{Z} \cdot (p \cdot r + o)^{p \cdot r + o} \cdot ((1-p) \cdot r + 1 - o)^{(1-p) \cdot r + 1 - o} \tag{15}
$$

with Z such that $\mathcal{L}(r|o=1) + \mathcal{L}(r|o=0) = 1$, that is Equation 11.

8.4.2 Python code

```python
def likelihood(o, p, r):
    """
    Knowing $p$ and $r$, the sufficient statistics of the beta distribution
        $B(\alpha, \beta)$ :
    $$
        alpha = p*r
        beta  = (1-p)*r
    $$
    the likelihood of observing o=1 is that of a binomial of

        - mean rate of choosing hypothesis "o=1" = (p*r + o)/(r+1)
        - number of choices where "o=1" equals to p*r+1

    since both likelihood sum to 1, the likelihood of drawing o in the set {0,
        1}
    is equal to

    """
    def L(o, p, r):
        P =  (1-o) * ( 1. - 1 / (p * r + 1) )**(p*r) * ((1-p) * r + 1)
        P +=  o * ( 1. - 1 / ((1-p) * r + 1) )**((1-p)*r) * (p * r + 1)
        return P
```

```
L_yes = L(o, p, r)
L_no = L(1-o, p, r)
return L_yes / (L_yes + L_no)
```

8.4.3 Properties

This function has some properties, notably symmetries:

- for certain outcomes, $\forall r > 0$, $\mathcal{L}(o|p = 0, r) = 1 - o$ and $\mathcal{L}(o|p = 1, r) = o$,
- if $r = 0$, the likelihood is uniform $\mathcal{L}(o) = 1/2$,
- $Pr(o|p, r) = Pr(1 - o|1 - p, r)$.

Note also that as r grows, the likelihood gets sharper.